Stellar Evolution and Nucleosynthesis:

Main Sequence and Post Main Sequence

by

Sanchari Sen

Roll No.: 107

Supervisors: Dr. Suparna Roychowdhury[1]

& **Prof. Dhruba Gupta**[2]

B.Sc (Honours)

Department of Physics

St. Xavier's College (Autonomous), Kolkata

"I affirm that I have identified all my sources and that no part of my dissertation paper uses unacknowledged materials."

[1] Assistant Professor, Department of Physics, St. Xavier's College (Autonomous), Kolkata

[2] Professor, Department of Physical Sciences, Bose Institute

Acknowledgements

It is said that the journey of a thousand miles begins with a single step. This is definitely one such step. This dissertation is a product of not just my research and review, but the collective efforts of some people I am forever grateful to have around me.

To begin with, I would like to express my sincere gratitude to my supervisors, Dr. Suparna Roychowdhury and Prof. Dhruba Gupta for their invaluable guidance and support throughout this entire process.
First and foremost, I am immensely grateful to Dr. Suparna Roychowdhury for her insights, ideas and expertise in planning out my dissertation and guiding me through each small and big step of it. Above all, her patience, particularly in navigating my missteps and, at times, unconventional ideas, has been truly exceptional.
I am equally grateful to Prof. Dhruba Gupta, for his constant guidance and ideas since the very beginning. Moreover, I thank him for allowing me to work at the Nuclear Astrophysics Lab, Bose Institute, Kolkata, one of the most prestigious research labs in India. His ideas and suggestions in helping me find the conjunction of nuclear physics and stellar astrophysics has been extraordinary. I would also like to thank Bose Institute for allowing me to access their facilities and successfully complete my work.

Moreover, I'd like to thank all my professors in the department, the non-teaching staff and the entire administration of the college. I'd especially like to thank Mr. Bappaditya Manna, Technical Officer, Father Eugene Lafont Observatory (FELO), for his help and support.

To the supporters behind the curtains, I probably could not have completed this work without my seniors Rupam Jash (Paris Observatory, PSL), Dr. Kabita Kundalia and Ritankar Mitra (Bose Institute). In spite of their immensely busy schedule and very different lines of research they hand-held me through all the major steps while handling all my carelessness with patience. All of the nuclear physics computations would have been an unsolvable puzzle for me if not for Kabita di and Ritankar da. Rupam da's constant push and discussions and proofreads since before the start of this journey have brought it here today. Dissertation discussions would not have been half as interesting without my project partners, Uditi and Soumik. Even though my work has been totally different from theirs, they were never short of support and enthusiasm. I am also thankful to my friends- at SXC and beyond, and some wonderful juniors for their feedback and most importantly encouragement in this work.

Finally, the people who made it possible for me to reach this far- my family. It's easier to guide a young mind but much more difficult to be patient and trustful as they carve their own ways. I will forever be indebted to them for everything so far, and beyond.

Thank you everyone for making this a "stellar" adventure!

Abstract

Stars are natural laboratories for elemental synthesis, shaping galaxies and the universe. Their evolution, from the Main Sequence (MS) to post-MS phases, is driven by nuclear reactions that influence their structure, mass, and composition. Elements beyond lithium originate through stellar nucleosynthesis, making its study crucial. This thesis explores post-MS nuclear reactions, including triple-alpha capture and the "holy grail," focusing on reaction rate calculations. Additionally, we analyze stellar surveys (GAIA, SDSS, HIPPARCOS) to construct color-magnitude diagrams and track stellar evolution. By studying stellar clusters, we identify coeval stars and MS turnoff points. We also examine MS stellar evolution models, emphasizing the role of initial mass in determining stellar properties. Future work will further explore the link between stellar masses and nucleosynthesis through exploring reactions in detail and more evolutionary models.

Contents

List of Figures

CHAPTER 1

Introduction

"We are made out of stardust. The iron in the haemoglobin molecules in the blood in your right hand came from a star that blew up 8 billion years ago. The iron in your left hand came from another star." *-Jill Tarter*

Astronomy is regarded as the oldest of natural sciences, with its roots dating back to the earliest civilizations, when positions of celestial bodies in the sky served as a guide to navigation, making calendars, and many more. Following the Renaissance era of Kepler and Newton, stellar astrophysics was born when William Herschel laid the foundation of stellar statistics and developed his theory of *Cosmogony* [16], while Kirchhoff and Bunsen revealed that stars are composed of elements found on earth. Eddington became a pioneer in the physics of stars [17] in 1926 by predicting the role of the nuclear process in stellar evolution [18] while Bethe, 13 years later, explained the exact fusion process [19]. Since then stellar physics became a product of advanced understanding in nuclear physics and a revolution in big data by large observational projects. While by 1953, Hoyle predicted a carbon-12 resonance to allow stellar triple alpha reactions, ESA launched Hipparcos in 1989- stepping into the big data period of stellar astronomy.

Today, in the big data age, observational projects like GAIA and SDSS are goldmines of stellar data, while the nuclear physics behind stellar evolution is under study through facilities like ISOLDE, CERN, and SPIRAL1, GANIL.

This dissertation is an attempt to examine the observational and theoretical aspects of stellar evolution and structure, by studying evolutionary models against observational data and understanding the role of nucleosynthesis in Main Sequence (MS) and Post-Main Sequence stars. Stars begin their evolution in the MS phase, fusing hydrogen into helium in their cores, which emits energy and causes them to shine. As core hydrogen depletes, it enters the Post-Main Sequence phase, undergoing significant structural and dynamic changes driven by core nuclear reactions. These processes alter their mass and chemical composition, leading to the creation of elements heavier than lithium through stellar nucleosynthesis. Understanding stellar evolution provides crucial insights into the origins and abundances of elements that form planets and life.

The study is organized as follows: In the first section, we begin with an introduction to stellar evolution and nucleosynthesis, which it explores stellar physics, covering spectral classification and HR diagrams, stellar structure modeling in general, and energy generation through nuclear processes. Next, it discusses Main Sequence modeling, including the role of the pp chain and CNO cycle, theoretical homologous models, and computational methods like StatStar. The study then tests these models against star survey data, analyzing observational datasets. Post-Main Sequence evolution is examined through nucleosynthesis and R-Matrix analysis. It concludes with key findings, followed by appendices detailing data analysis using GAIA DR3 and HIPPARCOS, along with case studies on Aquarius and Virgo stars.

CHAPTER 2

Stellar Physics

2.1 Spectral Classification and HR Diagram

The Spectral Types of Stars

When starlight is dispersed into its constituent wavelengths, it produces a stellar spectrum—a pattern of alternating dark and bright lines. These spectral lines act as unique fingerprints, revealing lots of information about a star's temperature, density, and chemical composition. While stellar spectra are influenced by both temperature and surface gravity, temperature plays the dominant role. Given that the chemical compositions of most stars are broadly similar, spectral classification serves as a powerful tool to arrange stars in a sequence of decreasing temperatures. This ordering is achieved by analyzing the specific spectral lines present, which directly correlate with the star's atmospheric temperature.

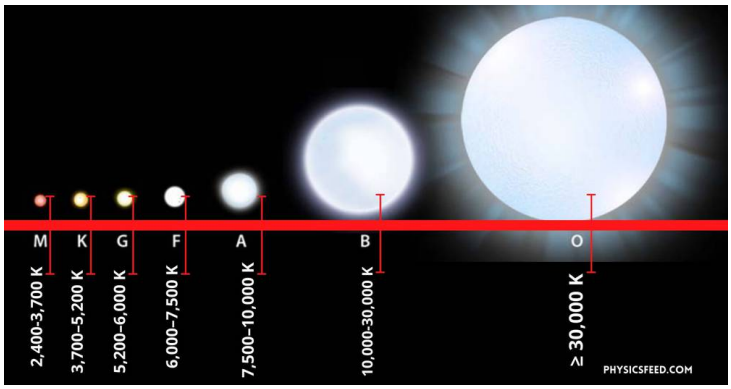

Figure 2.1: Harvard Spectral Classification of Stars [6]

Stars are primarily classified using the Harvard Classification Scheme: OBAFGKM, from hottest (O) to coolest (M). Each class is subdivided 0-9, with 0 hottest (e.g., A8, A9, F0, F1). Stars towards O are 'early-type', those towards M are 'late-type'.

Origin of Spectral Lines

The spectral lines are formed by different ionization and excitation states of the atoms in the stellar atmosphere due to different temperatures.
The **Boltzmann equation** describes the relative population of different energy levels within an atom at a given temperature. It tells us how many atoms of a particular element will have their electrons in a specific energy level.

$$\frac{N_j}{N_i} = \frac{g_j}{g_i} e^{-\frac{E_j - E_i}{kT}}$$

Thus, at higher temperatures, a larger fraction of atoms will be in higher energy levels. For an absorption line to be strong, a significant number of atoms must be in the lower energy level of the transition. As temperature changes, the population of these levels changes, leading to variations in the strength of the corresponding absorption lines.
The **Saha equation** describes the degree of ionization of an element as a function of temperature and pressure (electron density). It tells us the ratio of the number of ions in one ionization state to the number of atoms in the next lower ionization state.

$$\frac{N_{i+1}}{N_i} = \frac{2kTZ_{i+1}}{P_e Z_i} \left(\frac{2\pi m_e kT}{h^2} \right)^{3/2} \exp\left(-\frac{\chi_i}{kT} \right)$$

So, at higher temperatures, atoms are more likely to be ionized.
The strength of an absorption line for a particular transition in an atom of a specific element depends directly on the number density of those atoms that are in the initial energy level of that transition.

- The **Saha Equation** can tell us the ratio of singly ionized atoms (N_{i+1}) to neutral atoms (N_i) of a given element at a specific temperature and pressure.

  $$N_{\mathrm{n}}(X) = f_{\mathrm{n}}(T, P_e) \ddot{\mathrm{O}} N_{total}(X)$$

  where $N_{\mathrm{n}}(X)$ is the number density of element X in neutral state, $N_{total}(X)$ is the total number density of element X, and $f_{\mathrm{n}}(T, P_e)$ the fraction of atoms in neutral state at specific temperature and pressure.

- The **Boltzmann equation** gives the ratio of the number density of atoms in level i (N_i) to the number density in some reference level.

  $$\frac{N_i}{N_{\mathrm{n}}(X)} = \frac{g_i}{Z_{\mathrm{n}}(T)} \exp\left(-\frac{(E_i - E_1)}{kT} \right)$$

  and

  $$N_i = f_{\mathrm{ex}}(T) N_{\mathrm{n}}(X)$$

Combining the Boltzmann and Saha Equation, we get

$$N_i = f_{\mathrm{ex}}(T) f_{\mathrm{n}}(T, P_e) N_{\mathrm{total}}(X)$$

By theoretically calculating the expected strengths of these lines as a function of temperature and pressure using the combined Boltzmann and Saha equations (and detailed models of stellar atmospheres), and then comparing these predictions to the observed spectrum, astronomers can determine the star's surface temperature and thus its spectral classification [1].

HR Diagram

The Hertzsprung–Russell diagram shows absolute magnitude or luminosity of stars varies against colour or effective temperature. A star undergoes a sequence of evolutionary phases governed by its internal structure and energy production mechanism, both of which are primarily determined by its initial mass. During these phases, the star experiences changes in temperature and luminosity, leading to its progression across different regions of the Hertzsprung-Russell (HR) diagram. So if we can locate a star on the HR diagram, we can identify its internal structure and stage of evolution.

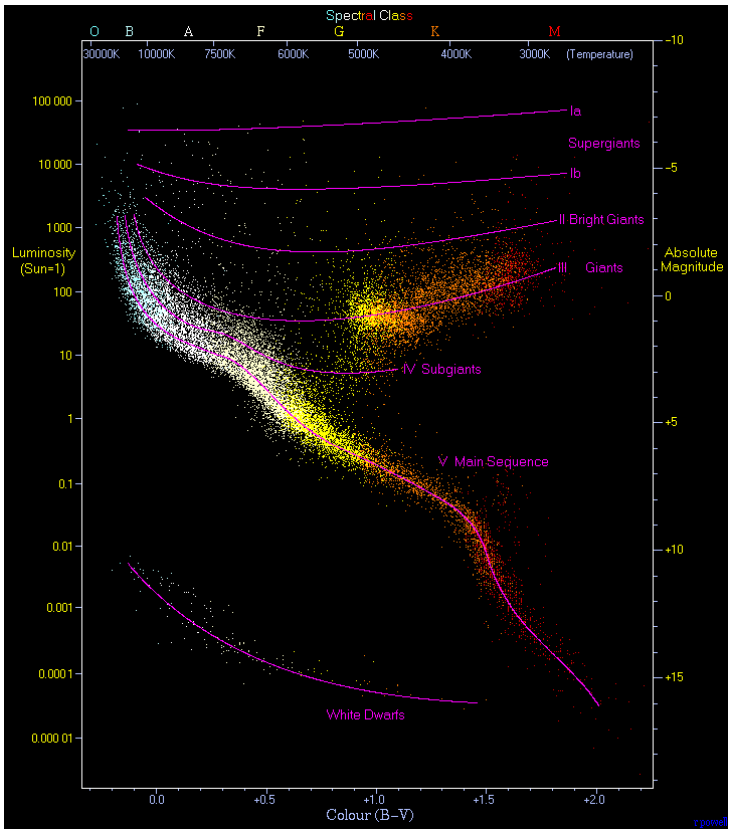

Figure 2.2: Hertzsprung–Russell diagram with 22,000 stars plotted from the Hipparcos Catalogue and 1,000 from the Gliese Catalogue of nearby stars.[7]

The HR diagram has the primary regions as follows:

1. The *main sequence*, taking up the majority, goes roughly from faint red to bright blue. More than 90% of the life of a star is spent here, where hydrogen is converted to helium at their core.

2. Red giants and supergiants lie above the main sequence. By the Stefan-Boltzmann law, their low temperatures and high luminosities mean large radii. This stage begins when a star depletes its core hydrogen and starts to burn heavier elements.

3. In the lower-left corner of the HR diagram, there are low to intermediate-mass stars and white dwarf stars, the ultimate evolutionary stage. These stars' low luminosities are a result of their small size, although they are extremely hot.

2.2 Modeling the Structure of Stars

Mass Conservation

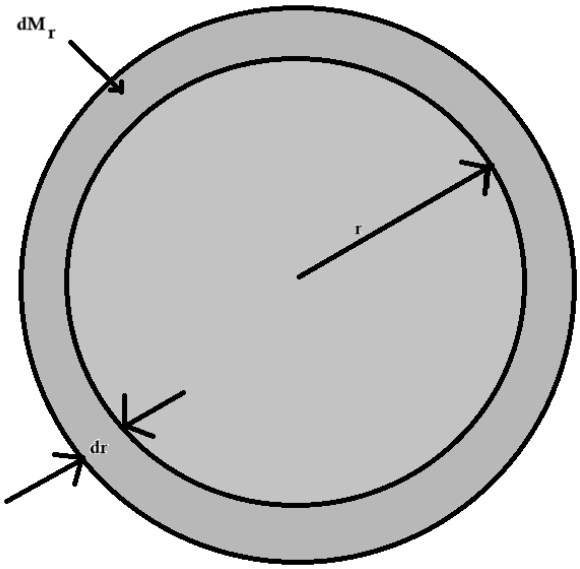

Figure 2.3: A spherically shell of mass dM_r and density ρ

Consider a shell of mass dM_r and thickness dr in a spherically symmetric star, at a distance r from the centre of the star. Assuming $dr << r$, i.e. the shell is sufficiently thin, it is $dV = 4\pi r^2 dr$. If the local gas density is ρ, the shell's mass is given by

$$\begin{aligned} dM_r &= 4\pi r^2 \rho \, dr \\ \implies \frac{dM_r}{dr} &= 4\pi r^2 \rho \end{aligned}$$

This is the equation of mass conservation [1].

Hydrostatic Equilibrium

As the gravitational force is always attracting, a star needs an opposing force to prevent collapse. Pressure provides this force. Consider a cylinder of mass dm whose base is placed at a distance r from the centre of a spherical star to determine how the pressure must change with depth.

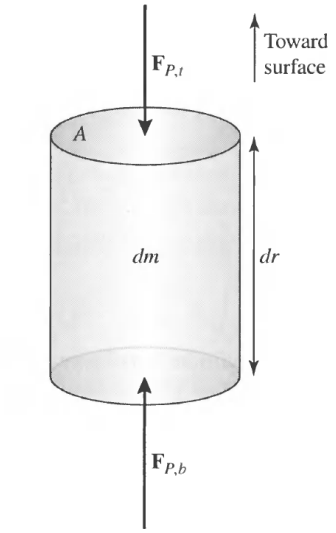

Figure 2.4: In a static star the gravitational force on a mass element is exactly canceled by the outward force due to a pressure gradient in the star. [1]

The cylinder's areas at its top and bottom are each A, and its height is dr. Also, consider that the pressure force, which is always normal to the surface and may change depending on how far the cylinder is from the star's centre, and gravity are the only forces acting on the cylinder.

By Newton's Second Law,

$$\vec{F} = m.\vec{a}$$

now,

$$\vec{F} = \vec{F_g} + \vec{F_{p,t}} + \vec{F_{p,b}}$$
$$\therefore dm\frac{d^2\vec{r}}{dt^2} = \vec{F_g} + \vec{F_{p,t}} + \vec{F_{p,b}}$$

When $F_{p,t}$ is expressed in terms of $F_{p,b}$ and a correction term dF_p that takes into account the change in force brought on by a change in r, the resulting expression is

$$F_{p,b} = -(F_{p,t} + dP_p)$$

So the previous equation becomes

$$dm\frac{d^2m}{dt^2} = F_g + dF_p$$

where $F_g = -\dfrac{GM_r dm}{r^2}$, M_r being the mass inside the sphere of radius r, often referred to as the interior mass. Also,

$$P = \frac{F_p}{A}$$

$$\implies dF_p = AdP$$

If the density of the gas in the cylinder is ρ, its mass is

$$dm = \rho A dr$$

. So substituting in the above equation, we get

$$\rho A dr \frac{d^2r}{dt^2} = -\frac{GM_r \rho A dr}{r^2} - AdP$$
$$\implies \rho \frac{d^2r}{dt^2} = -\frac{GM_r \rho}{r^2} - \frac{dP}{dr}$$

The acceleration must be 0 if we further assume that the star is static. So the equation becomes

$$\frac{dP}{dr} = -\frac{GM_r \rho}{r^2} = -\rho g$$

where g is the local acceleration due to gravity at radius r. So the above equation satisfies the condition of **hydrostatic equilibrium** [1].
Multiplying the denominator on both sides of the above equation by $4\pi r^2 \rho$, we get

$$\frac{dP}{(4\pi r^2 \rho) dr} = -\frac{GM_r \rho}{(4\pi r^2 \rho) r^2}$$
$$\therefore \frac{dP}{dm} = -\frac{GM_r}{4\pi r^4}$$

This is another form of hydrostatic equilibrium with dependence on the stellar mass and represents one of the fundamental equations of stellar structure for spherically symmetric objects.

Power conservation

The star at its core is powered by all the energy produced by the stellar material. This can be established from the star's luminosity profile. Given an infinitesimal mass dm, the contribution to the overall luminosity is

$$dL = \epsilon dm$$

where ϵ is the total energy released per kilogram per second by all nuclear reactions and by gravity, or $\epsilon = \epsilon_{\text{nuclear}} + \epsilon_{\text{gravity}}$. The mass of a shell of a spherically symmetric star is $dM_r = \rho dV = 4\pi r^2 \rho dr$. Substituting in the equation if dL, we get

$$\frac{dL_r}{dr} = 4\pi r^2 \rho \epsilon$$

where L_r denotes the internal luminosity resulting from all of the energy produced inside the star's interior out to radius r [1].

Energy Transport

We can assume that radiation moves in straight lines (called rays) through space or homogeneous media when the scale of a system substantially exceeds the wavelength of radiation. The

theory governing all these transfer phenomena can be chalked: *Theory of Radiative Transfer*. Consider an element of area dA that has been exposed to radiation for a period of time dt. The amount of energy passing through the element should be proportional to dAdt, and we write it as FdAdt where F is the energy flux [1].

If we consider a spherically symmetric isolated source (for example, an isolated star) of radius r, the energy flux is

$$F(r) = \frac{C}{r^2}$$

where C=constant.
The energy per unit volume per unit frequency range is referred to as the specific energy density, u_ν. If mean intensity $J_\nu = \frac{1}{4\pi}\int I_\nu d\Omega$ (where I_{nu} is the intensity of radiation), we can write

$$u_\nu = \frac{4\pi}{c} J_\nu$$

So the **total radiation density** is

$$u = \int u_\nu d\nu = \frac{4\pi}{c}\int J_\nu d\nu$$

If we consider an isotropic radiation field contained in a reflecting enclosure, then each photon transfers twice its normal component of momentum on reflection. So we can say

$$p_\nu = \frac{2}{c}\int I_\nu \cos^2(\theta) d\Omega$$

Since the radiation is isotropic, $I_\nu = J_\nu$, so

$$p = \frac{2}{c}\int J_\nu d\nu \int \cos^2(\theta) d\Omega = \frac{1}{3}u$$

So the **radiation pressure** of an isotropic radiation field is one-third of its energy density.

To achieve the **Radiative Transport Equation for Stellar Interiors**, we use the general radiative transfer equation (RTE):

$$\frac{dI_\nu}{ds} = -\kappa_\nu \rho I_\nu + j_\nu$$

where:

- I_ν is the specific intensity at frequency ν.
- s is the path length.
- κ_ν is the opacity at frequency ν.
- ρ is the density.
- j_ν is the emissivity at frequency ν.

In a spherically symmetric star (r, θ, ϕ), the path length ds is:

$$ds = \frac{dr}{\mu}$$

where $\mu = \cos\theta$.
Substituting $ds = dr/\mu$ into the general RTE,

$$\mu \frac{dI_\nu}{dr} = -\kappa_\nu \rho I_\nu + j_\nu$$

Now, source function $S_\nu = \frac{j_\nu}{\kappa_\nu \rho}$, so, taking the first moment to get the flux:

$$\mu \frac{dI_\nu}{dr} = -\kappa_\nu \rho (I_\nu - S_\nu)$$

The mean intensity $J_\nu = \frac{1}{2}\int I_\nu d\mu$
Radiative flux

$$F_\nu = 2\pi \int I_\nu \mu d\mu$$

To find the variation of pressure, we take integral over all solid angles, weighted by μ (second moment):

$$\int \mu^2 \frac{dI_\nu}{dr} d\mu = \int -\kappa_\nu \rho (I_\nu - S_\nu)\mu d\mu$$
$$\implies \frac{d}{dr}\left(\frac{1}{2}\int I_\nu \mu^2 d\mu\right) = -\kappa_\nu \rho \left(\frac{1}{2}\int I_\nu \mu d\mu - \frac{1}{2}\int S_\nu \mu d\mu\right)$$

For spherical symmetry, if S_ν is isotropic, $\int S_\nu \mu d\mu = 0$. Using $P_\nu = \frac{2\pi}{c}\int I_\nu \mu^2 d\mu$:

$$\frac{1}{4\pi}\frac{dP_\nu}{dr} = -\frac{\kappa_\nu \rho}{4\pi} F_\nu$$

Defining $P_r = \int_0^\infty P_\nu d\nu$ and $F = \int_0^\infty F_\nu d\nu$:

$$\frac{dP_r}{dr} = -\frac{\kappa \rho}{c} F$$

This gives the variation of pressure, as we move to the interior of a star.
To find the variation of pressure, we take the integral over all solid angles:

$$\int \mu \frac{dI_\nu}{dr} d\mu = \int -\kappa_\nu \rho (I_\nu - S_\nu) d\mu$$
$$\implies \frac{d}{dr}\left(\frac{1}{2}\int I_\nu \mu d\mu\right) = -\kappa_\nu \rho \left(\frac{1}{2}\int I_\nu d\mu - S_\nu\right)$$
$$\implies \frac{1}{4\pi}\frac{dF_\nu}{dr} = -\kappa_\nu \rho (J_\nu - S_\nu)$$

This gives the variation of flux, as we move to the interior of a star.

We can relate the radiative flux to the gradient of the mean intensity at the deep interior of the star using the diffusion approximation:

$$F_\nu = -\frac{4\pi}{3\kappa_\nu \rho}\frac{dJ_\nu}{dr}$$

Integrating over all frequencies for the flux variation:

$$\frac{1}{4\pi}\frac{dF}{dr} = \int_0^\infty -\kappa_\nu \rho (J_\nu - S_\nu) d\nu = \rho\epsilon$$

where ϵ is the energy generation rate per unit mass.

Combining $F = -\frac{4\pi}{3\kappa\rho}\frac{dJ}{dr}$ with $\frac{dP_r}{dr} = -\frac{\kappa\rho}{c}F$ and using $J = acT^4/(4\pi)$ and $P_r = acT^4/3$:

$$F = -\frac{4\pi r^2 acT^3}{3\kappa\rho}\frac{dT}{dr}$$

Finally, the radiative transport equation in spherical symmetry:

$$\frac{dT}{dr} = -\frac{3\kappa\rho}{4acT^3}\frac{L}{4\pi r^2}$$

where:

- T is the temperature.
- L is the luminosity.
- a is the radiation constant.
- c is the speed of light.
- κ is the Rosseland mean opacity.

Stellar Structure Equations

The basic time-independent (static) stellar structure equations are summarized below [1]:

$$\boxed{\begin{aligned}\frac{dM_r}{dr} &= 4\pi r^2 \rho, \\ \frac{dP}{dr} &= -\frac{GM_r\rho}{r^2}, \\ \frac{dL_r}{dr} &= 4\pi r^2 \rho\epsilon, \\ \frac{dT}{dr} &= -\frac{3\kappa\rho}{4acT^3}\frac{L}{4\pi r^2}\end{aligned}}$$

The complementary equations are the equations of state of the material and are collectively referred to as constitutive relations. We require relationships for the pressure, opacity, and energy generation rate in terms of the density, temperature, and composition of the material, specifically:

$$\boxed{\begin{aligned} P &= \frac{R}{\mu_1}\rho T + P_e + \frac{1}{3}aT_4 \\ \kappa &= \kappa_0\, \rho^{\,a}\, T^{\,b}, \\ \epsilon &= \epsilon_0\, \rho^{\,m}\, T^{\,n} \end{aligned}}$$

To obtain actual solutions of stellar structure equations, we require proper boundary conditions. The conditions for the core are:

$$\left.\begin{aligned} M_r &\to 0, \\ L_r &\to 0 \end{aligned}\right\} \quad \text{as } r \to 0$$

The conditions for the surface of the star are:

$$\left.\begin{aligned} T &\to 0, \\ p &\to 0, \\ \rho &\to 0 \end{aligned}\right\} \quad \text{as } R \to R_\star$$

Virial Theorem and Mass Average Temperature

An important consequence of hydrostatic equilibrium is a link that it establishes between gravitational potential energy and internal energy (or kinetic energy in a system of free particles) of a self-gravitating system, in our case, a star.
From the equation of hydrostatic equilibrium,

$$dP = -\frac{GM_r}{4\pi r^4} dm$$

Multiplying both sides by volume $V = \frac{4}{3}\pi r^3$, we get

$$VdP = -\frac{GM_r}{4\pi r^4}\, dm\, \frac{4}{3}\pi r^3$$

and integrating over the whole star, we get,

$$\int_0^{P(R)} VdP = -\frac{1}{3}\int_0^M \frac{GM_r dm}{r}$$

The integral on the right-hand side of the equation is the gravitational potential energy of the star, that is, the energy required to assemble the star by bringing matter from infinity,

$$\Omega = -\frac{1}{3}\int_0^M \frac{GM_r dm}{r}$$

The left hand side becomes $[PV]_0^R - \int_0^{V(R)} PdV$. V=0 at the centre of the star and V=0 at the surface, so $[PV]_0^R \longrightarrow 0$. Also, $dV = \frac{dm}{\rho}$. Substituting everything, we get

$$-3\int_0^M \frac{P}{\rho}\, dm = \rho$$

. Thus we get the global form of the **Virial Theorem**.

Now using Virial Theorem, we can find the mass average temperature of a Main Sequence Star. Consider an ideal gas of density ρ and temperature T (we assume the star to be formed of an ideal gas). If the mass of the gas particles b m_g, the pressure P becomes $P = \frac{\rho}{m_g} kT$. The kinetic energy per particle is $\frac{3}{2} kT$.
The internal energy of an ideal gas is its kinetic energy. So the internal energy per unit mass is

$$\begin{aligned} u =& \frac{3kT}{2m_g} = \frac{3P}{2\rho} \\ \implies \frac{P}{\rho} =& \frac{2}{3} u \end{aligned}$$

Using virial theorem, we have

$$\begin{aligned} -3 \int_0^M \frac{2u}{3} dm =& \Omega \\ \implies \int_0^M u \, dm =& -\frac{1}{2}\Omega = U \end{aligned}$$

U being the total internal energy. The gravitational potential Ω is given by $\Omega = -\alpha \frac{GM_r^2}{R}$, (R being the radius of the star) where α is determined by the star's density profile, and gives the distribution of matter within the star. From the equation

$$\begin{aligned} u =& \frac{3\,kT}{2\,m_g} \\ \implies \int_0^M u \, dm =& \int_0^M \frac{3\,kT}{2m_g} dm \\ \implies U =& \frac{3\,kTM_r}{2m_g} \\ \implies -\frac{1}{2}\,\Omega =& \frac{3\,kTM_r}{2\,m_g} \\ \implies \frac{\alpha\, GM_r^2}{2R} =& \frac{3\,kTM_r}{2\,m_g} \\ \therefore \overline{T} =& \frac{\alpha}{3} m_g \frac{GM_r}{kR} \end{aligned}$$

Thus $\overline{T}$ is the average internal energy of a star.
If the average density of a star (considering it uniform), $\overline{\rho} = \frac{3M}{4\pi R^3}$, then we have

$$\overline{T} = \frac{\alpha}{3} \frac{MG\, m_g}{k} \left(\frac{3M}{4\pi \overline{\rho}} \right)^{-1/3}$$

$$\implies \overline{T} \propto M^{\,2/3}\, \overline{\rho}^{\,1/3}$$

So if two stars have the same mass, the denser one is hotter. Writing the equation of the average

internal temperature of stars in terms of solar constants, we get

$$\overline{T} = \frac{\alpha}{3}\frac{m_g}{k}\frac{G}{}\frac{M_\odot}{R_\odot}\left(\frac{M}{M_\odot}\right)\left(\frac{R_\odot}{R}\right)$$

Putting in all the values and keeping $\alpha = 1/2$ for atomic hydrogen, we get

$$\overline{T} \approx 4 \times 10^6 \times \left(\frac{M}{M_\odot}\right)\left(\frac{R_\odot}{R}\right) K$$

This is the average temperature of a main sequence star like the sun. The temperature near the core is of the order of 10^7 K while the surface temperature is about 5772 K. Thus the virial temperature allows us to obtain the average temperature of a star without using any stellar model [2].

2.3 Energy Generation through Nucleosynthesis

Timescales in stellar evolution

Each process in stellar evolution has a characteristic timescale *tau*, the ratio of the quantity changed by the process with the rate of change

$$\tau = \frac{\phi}{\dot{\phi}}$$

1. The Dynamical timescale- This corresponds to a change in the physical structure of a spherically symmetric star when the gravitational force is not balanced by the pressure forces.

$$\tau_{\text{dynamical}} = \frac{R}{\dot{R}} = \frac{R}{v_{\text{esc}}} = \frac{R}{\sqrt{2GM/R}} = \sqrt{\frac{R^3}{2GM}}$$

$$\bar{\rho} = \frac{3M}{4\pi R^3}$$

Putting this is in the equation of $\tau_{\text{dynamical}}$, we get

$$\therefore \tau_{\text{dynamical}} \approx \frac{1}{\sqrt{G\bar{\rho}}}$$

For the sun, this is about 1000 seconds, so we can write

$$\therefore \tau_{\text{dynamical}} \approx 1000\sqrt{\left(\frac{R}{R_\odot}\right)^3\left(\frac{M_\odot}{M}\right)}\text{secs}$$

2. The Thermal timescale- It is the time that would take a star to emit its entire reserve of thermal energy upon contraction, provided it maintains a constant luminosity. This is also known as the Kelvin-Helmholtz timescale. Here $\phi = U = GM^2/R$ and $\dot{\phi} = L$.

$$\therefore \tau_{\text{th}} = \frac{U}{L} = \frac{GM^2}{RL}$$

For the sun, this is $10^{15}s \approx 30$ million years $< 1\%$ of the star's lifespan. If a star maintains thermal and hydrostatic equilibrium during its evolutionary phase, its total energy is constant.

3. The Nuclear timescale- The time that a star spends on the main sequence – essentially the duration of the star's nuclear fuel under a constant burn rate. Assuming thermal equilibrium, such that $L_{\text{nuc}} = L$,

$$\tau_{\text{nuc}} = \frac{\phi}{\dot{\phi}} = \frac{\epsilon Mc^2}{L_{\text{nuc}}} = \frac{\epsilon Mc^2}{L}$$

In solar units,

$$\tau_{nuc} \approx \epsilon(45) \times 10^{20} \left(\frac{M}{M_\odot}\right) \left(\frac{L_\odot}{L}\right) secs$$

which is much more than the estimated age of the universe [2].

Fusion in Main sequence

In main sequence stars (the Sun for example), the temperature of the interior is of the order of $10^7 K$. The mass average temperature is roughly $4 \times 10^6 K$ for the Sun. For fusion reactions to take place, this temperature should be sufficient to produce energy greater than the proton-proton potential barrier. Calculating the potential barrier height,

$$V = \frac{Z_A . Z_B e^2}{4\pi\epsilon r}$$

For protons, $Z_A = Z_B = 1$, $r \approx 1.2 \times 10^{-15} m$

$$\therefore V = \frac{(1.602 \times 10^{-19})^2}{4\pi(8.854 \times 10^{-12})(1.2 \times 10^{-15})}$$

$$\implies V = 1.923 \times 10^{-13} J$$

Now for the energy to be produced at the core of the sun,

$$E = \frac{3}{2} kT$$

$$\implies E = \left(\frac{3}{2}\right)(1.3806 \times 10^{-23})(1.5 \times 10^7)$$

$$\implies E = 3.106 \times 10^{-16} J$$

So classically, nuclear fusion will not happen at the star's core since this energy is less than the potential barrier.

But in Quantum Mechanics, a wave will only be restricted to cross a potential barrier if the barrier is infinite. Else there is always a non-zero probability that the wave will 'tunnel' through the barrier. This process is called *Quantum Tunnelling*. Now considering the wave-particle duality and Heisenberg's Uncertainty Principle, one proton can tunnel through and find itself in the central potential field of the other proton. This is how the protons in the stellar core

tunnel through and reach other protons for nuclear fusion to occur.

Basics of Fusion Interaction

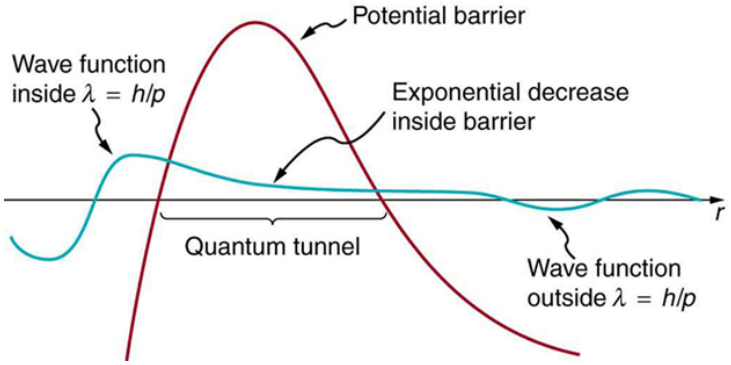

Figure 2.5: Mechanism of Quantum Tunnelling [8]

For a finite potential barrier, there is always a non-zero probability, that a particle will penetrate the barrier through tunnelling. If R_{nuc} is the nuclear radius where the particle will reach (i.e. the inner edge of the Coulomb barrier) and R_c is the classical radius (i.e. outer edge of the barrier), then the penetration probability is

$$P = \frac{|\Psi(R_{nuc})|^2}{|\Psi(R_c)|^2}$$

$$\implies P = \exp\left[-\left(\frac{E_G}{E}\right)^{1/2}\right]$$

where E is the particle energy and $E_G(= 2mc^2(\pi\alpha Z_A Z_B)^2)$ is the Gamow energy (α being the fine structure constant).

The probability of a nuclear reaction to occur is its **cross section** (σ). By definition,

$$\sigma(E) = \frac{S(E)}{E}\exp\left[-\left(\frac{E_G}{E}\right)^{1/2}\right]$$

where **S(E)** is called the **astrophysical S-factor** that includes all nuclear interactions.
We see that $\sigma(E)$ is very heavily dependent on energy of reaction. S(E) is weakly dependent on E and thus is a more reliable factor for extrapolation.

The **reaction rate** of a reaction is given by the reaction cross section and the relative velocity of the two nuclei fusing, given by

$$< \sigma v >= \int_0^\infty \sigma v P(v) dv$$

$$\implies < \sigma v >= \sqrt{\frac{8}{\pi m}}\left(\frac{1}{kT}\right)^{3/2}\int_0^\infty E.\sigma(E)\exp\left(-\frac{E}{kT}\right)dE$$

$$\implies < \sigma v >= \sqrt{\frac{8}{\pi m}} \left(\frac{1}{kT}\right)^{3/2} \int_0^\infty S(E) \exp\left(-\frac{E}{kT}\right) \exp\left[\left(-\frac{E_G}{E}\right)^{1/2}\right] dE$$

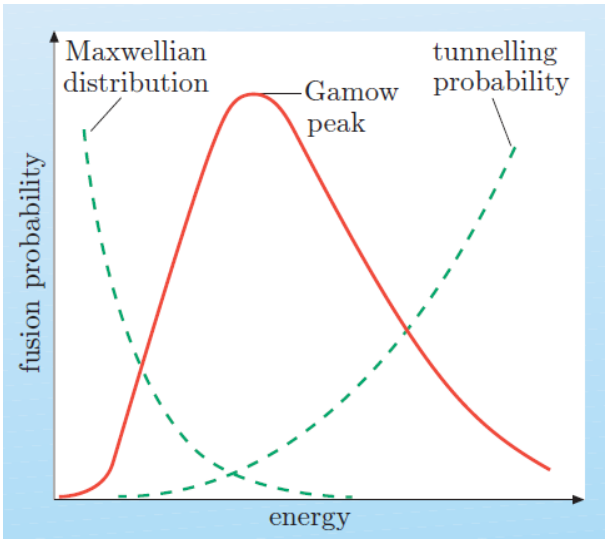

Figure 2.6: The Gamow peak in nuclear fusion.[3]

The product $\exp\left(-\frac{E}{kT}\right) \exp\left[\left(-\frac{E_G}{E}\right)^{1/2}\right]$ gives the Gamow peak. The Gamow peak is basically the product of the Maxwellian distribution and tunnelling probability. The area under the Gamow peak determines the reaction rate [3].

CHAPTER 3

Main Sequence Modeling

3.1 Nucleosynthesis in Main Sequence

The evolution of stars is due to their sustained emission of radiation originating from an internal source. This source is called stellar nucleosynthesis, where lighter elements transform into heavier ones under extreme temperature and pressure conditions. The main sequence nucleosynthesis is mainly governed by Hydrogen fusion when hydrogen burns at the core to produce helium. efficiency and dominant fusion reactions depend on factors like mass and core temperature, influencing the star's evolution. As nucleosynthesis progresses, the buildup of helium and other fusion byproducts gradually alters the star's internal composition, eventually leading to later stages of stellar evolution, where heavier elements are formed [2].

Hydrogen Burning

Hydrogen burning in the main sequence is characterised by two reaction sequences mainly: pp chain and CNO cycle. For stars with mass less than $1.5M_{\odot}$, pp chain reaction proceeds. For greater mass stars, the CNO cycle occurs.

The pp chain

The most abundant element being H (Z=1), two protons fuse by strong interaction of nuclear force and form He, but being highly unstable, it should break down immediately into two separate protons. But a way out of this was given by Bethe- an intermediate more stable isotope is formed. [2]

$$p + p \rightarrow {}^{2}D + e^{+} + \gamma$$

Baryon number, lepton number and charge are conserved in this. Then 2^D captures a proton and forms a lighter isotope of ${}^{3}He$:

$${}^{2}D + p \rightarrow {}^{3}He + \gamma$$

Now there can be three branches for the pp chain reaction to proceed:

$$
\begin{aligned}
(i) \quad \text{pp I chain} \quad &: \quad {}^3He + {}^3He \rightarrow {}^4He + 2p \\
(ii) \quad \text{pp II chain} \quad &: \quad {}^3He + {}^4He \rightarrow {}^7Be + \gamma \\
&\quad {}^7Be + e^- \rightarrow {}^7Li + \nu \\
&\quad {}^7Li + p \rightarrow 2\,{}^4He \\
(iii) \quad \text{pp III chain} \quad &: \quad {}^7Be + P \rightarrow {}^8B + \gamma \\
&\quad {}^8B \rightarrow {}^8Be + e^+ + \nu \\
&\quad {}^8Be \rightarrow 2\,{}^4He
\end{aligned}
$$

The transition from pp I to pp II occurs between temperatures of $1.3 \times 10^7 K$ to $2 \times 10^7 K$. and pp III dominates above $3 \times 10^7 K$.

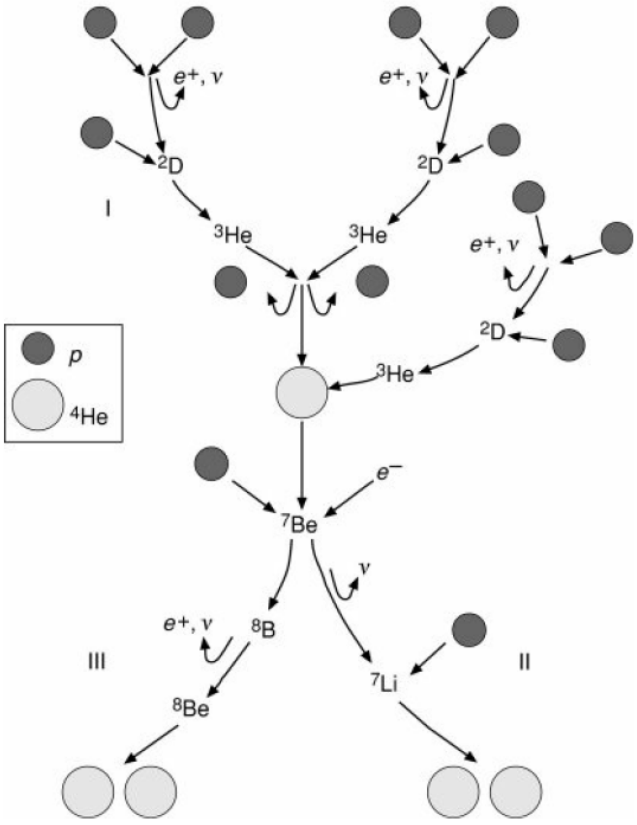

Figure 3.1: The nuclear reactions of the p-p I, II and III chains.[2]

The CNO cycle

A small fraction of a star's initial composition includes carbon, nitrogen, and oxygen (CNO) nuclei, which facilitate hydrogen fusion into helium through a catalytic cycle. This process, known as the CNO cycle, was independently proposed by Bethe and von Weizsäcker in 1938. The cycle consists of two interlinked reaction chains, each involving four proton captures and

two $\beta+$ decays, producing one helium-4 nucleus while maintaining a constant total abundance of CNO (and fluorine) nuclei. The burning rate is dictated by the slowest reaction, typically a proton capture, since β decays remain unaffected by external conditions. At extremely high temperatures, however, β decays can become the limiting step, slowing the process. The net energy released per helium nucleus is approximately 25 MeV after accounting for neutrino losses, and the energy generation rate follows a steep temperature-dependent power law. Alongside the proton-proton chain, the CNO cycle was instrumental in explaining stellar hydrogen burning, with Bethe playing a key role in both discoveries [2]. The CNO cycle can be shown as:

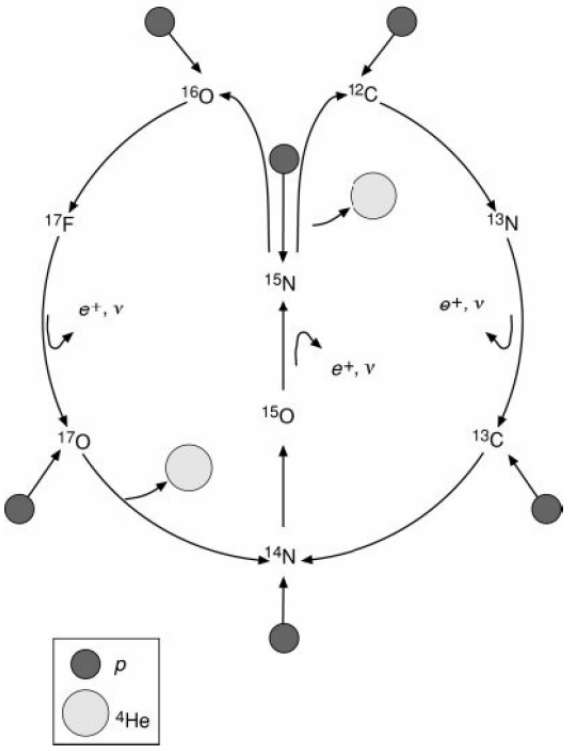

Figure 3.2: The nuclear reactions of the CNO cycle [2]

Density-Temperature plane: Stellar evolution

The evolution of a star is determined by the slowest reaction rate. The rates of burning increase with density and rise steeply with temperature. Since from the core outwards, temperature (T) and density (ρ) of a star falls, we say that stellar evolution is led by the core. So, T and ρ can determine the state of a star. The $\rho - T$ plane can be divided based on how the equations of state modify in various regions, or the phases of nuclear burning. [2]
From the common equation of state, $P = \frac{R}{\mu}\rho T = k_0 \rho T$, the pressure varies based on how T and ρ changes and we have the following zones:

- Ideal Gas
- Degeneracy

- Relativistic Degeneracy
- Radiation Pressure

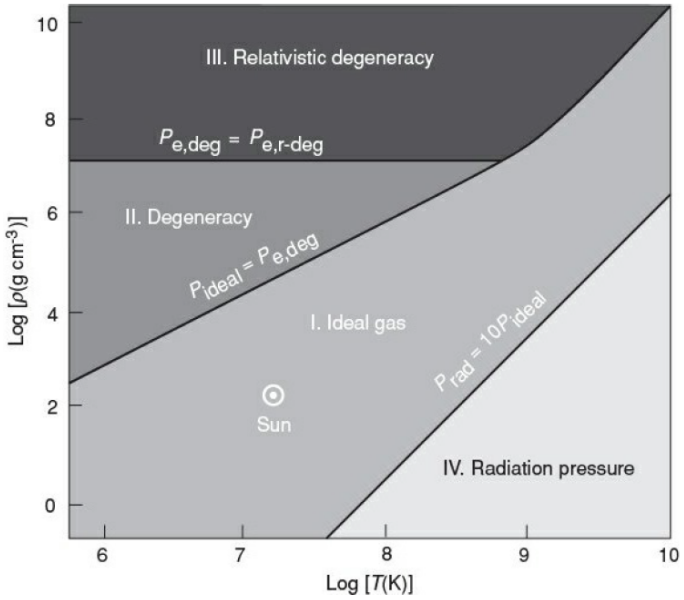

Figure 3.3: Mapping of the $\rho - T$ diagram according to the equation of state [2]

Stellar luminosities vary within a wide range but the variation in the conditions prevailing in burning zones is quite restricted, due to the high sensitivity of nuclear reaction rates to temperature. Hence a narrow threshold may be defined for each nuclear process that takes place in stars [2]. From the rate of reaction $\epsilon = \epsilon_0 \rho^m T^n$, the threshold of each zone is obtained from the limit $\epsilon = \epsilon_{min}$.

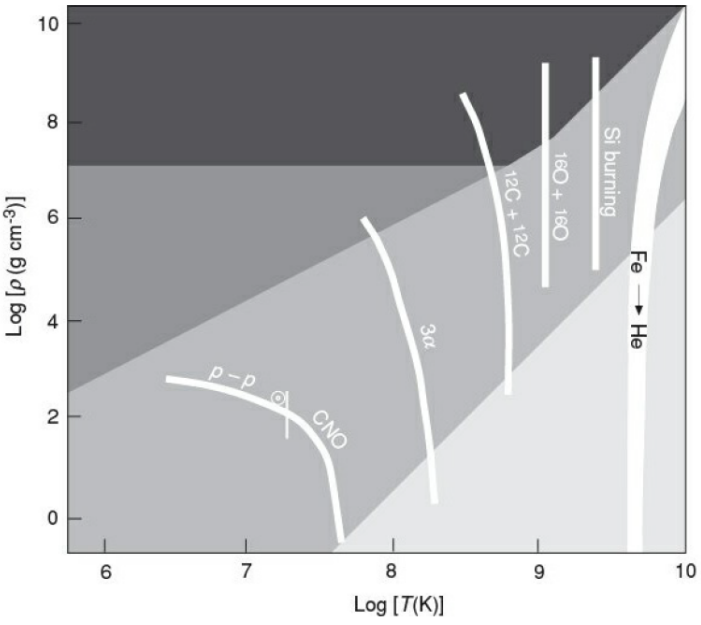

Figure 3.4: Mapping of the $\rho - T$ diagram according to the zones of nuclear burning [2]

3.2 Homologous Model

In the main sequence phase, hydrogen burning in the core is characterised by a pp chain reaction in lower-mass stars and a CNO cycle in higher-mass stars. The equation that governs this process is,

$$\log L = \alpha \log T_{eff} + \text{constant}$$

where α is the slope of the HR diagram. From the stellar structure equations :

$$\frac{dP}{dm} = -\frac{Gm}{4\pi r^4} \tag{3.1}$$

$$\frac{dr}{dm} = \frac{1}{4\pi r^2 \rho} \tag{3.2}$$

$$\frac{dT}{dm} = -\frac{3\kappa}{4acT^3}\frac{L}{(4\pi r^2)^2} \tag{3.3}$$

$$\frac{dL}{dm} = \epsilon \tag{3.4}$$

and the equation of state

$$P = \frac{R}{\mu}\rho \tag{3.5}$$

To solve these, let $x = \dfrac{m}{M}$

$$\implies dm = Mdx$$

Let

$$r = f_1(x)R_* \tag{3.6}$$
$$P = f_2(x)P_* \tag{3.7}$$
$$\rho = f_3(x)\rho_* \tag{3.8}$$
$$T = f_4(x)T_* \tag{3.9}$$
$$L = f_5(x)L_* \tag{3.10}$$

Putting (3.7) in (3.1) and separating, we get:

$$P_* = \frac{GM^2}{R_*^4} \tag{3.11}$$

and

$$\frac{df_2}{dx} = \frac{-x}{4\pi f_1^4}$$

Putting (3.6) in (3.2) and separating, we get:

$$\rho_* = \frac{M}{R_*^3} \tag{3.12}$$

and

$$\frac{df_1}{dx} = \frac{1}{4\pi f_1^2 f_3}$$

Similarly, putting (3.9) in (3.3) and separating, we get:

$$L_* = \frac{ac}{K}\left(\frac{T_*^4 R_*^4}{M}\right) \tag{3.13}$$

and

$$\frac{df_4}{dx} = \frac{3f_5}{4f_4^3(4\pi f_1^2)^2}$$

And, putting (3.10) in (3.4) and separating, we get:

$$F_* = M\rho_* T_*^n q_0 \tag{3.14}$$

and

$$\frac{df_5}{dx} = f_3 f_4^n$$

Finally, putting (3.7), (3.8) and (3.9) in (3.5) and separating, we get:

$$T_* = \frac{P_*\mu}{\rho_* R} \tag{3.15}$$

and

$$f_2 = f_3 f_4$$

Now we shall try to relate these major parameters with mass M.
Putting (3.12) in (3.15) and relating it to (3.13), we get a major relation

$$\boxed{L \propto \mu^4 M^3} \tag{3.16}$$

Equating (3.13) and (3.14), we get

$$\boxed{R_* \propto M^{\frac{n-1}{n+3}}} \tag{3.17}$$

Now using this (3.18) and (3.16),

$$\boxed{T_* \propto M^{\frac{4}{n+3}}} \tag{3.18}$$

And again using (3.18) on (3.12), we get

$$\boxed{\rho_* \propto M^{2(3-n)/(n+3)}} \tag{3.19}$$

Thus using the stellar structure equations we arrive at the above relations from (3.17) to (3.20).

Now applying the relation between luminosity and effective temperature $L = 4\pi R^2 \sigma T_{eff}^4$ on (3.17) and (3.18), we finally get

$$L^{1-\frac{2(n-1)}{3(n-3)}} \propto T_{\text{eff}}^4 \tag{3.20}$$

This is the equation for the Main Sequence phase.

For hydrogen burning, the pp chain has n=4. Putting n=4 and taking log on both sides,

$$\boxed{\log L = 5.6 \log T_{eff} + \text{constant}} \tag{3.21}$$

For the CNO cycle, putting n=16 and taking log on both sides,

$$\boxed{\log L = 8.4 \log T_{eff} + \text{constant}} \tag{3.22}$$

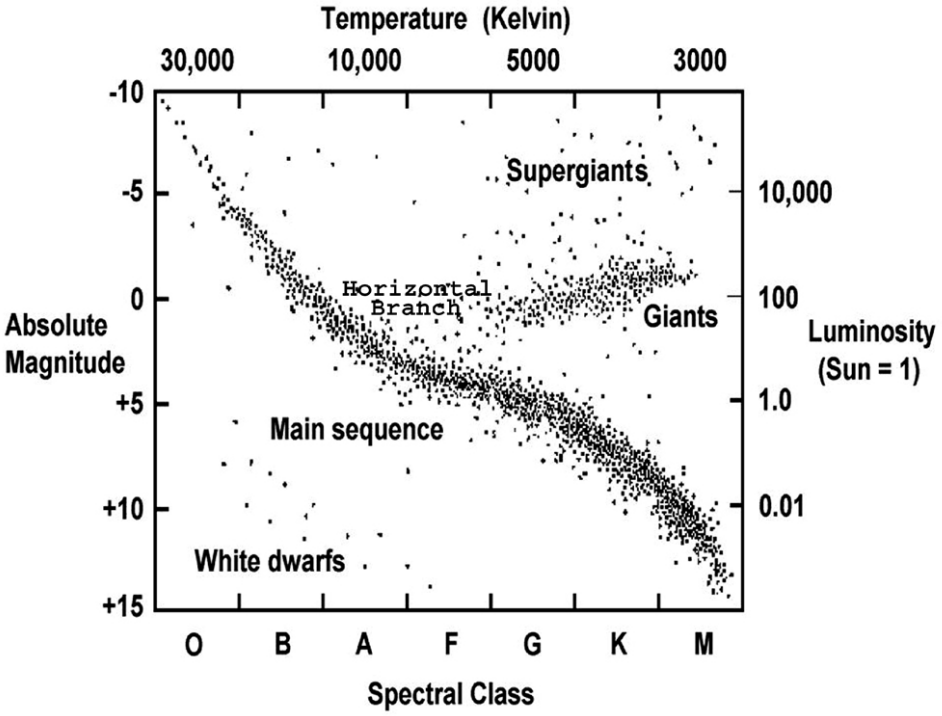

Figure 3.5: The main sequence phase in the HR Diagram [5]

In the main sequence branch, the curve is steeper in the upper region with higher mass (n=16) than the lower region with lower mass stars (n=4). This is also derived observationally in main sequence stars.

Minimum mass and luminosity for pp chain and CNO cycle

The nuclear energy reservoir of a star is proportional to its mass M. Also the rate of consumption of nuclear fuel is equal to the rate of energy release L in thermal equilibrium. So the duration of the main sequence phase is $\tau_{MS} = \frac{M}{L} = M^{-2}$. So the larger the stellar mass, the less time the star spends in the main sequence phase [2].

For pp chain:

We know $T \propto M^{\frac{4}{n+3}}$
For pp chain, n= 4 and the minimum temperature required $= T_{min} \approx 4 \times 10^6 K$
So, $T_C \geq T_{min}$ and $T_C \propto M^{4/7}$

Taking the ratio of the minimum temperature and central temperature of the sun and using it with solar mass, we get

$$\frac{M_{min}}{M_\odot} = \left(\frac{T_{min}}{T_{C,\odot}}\right)^{7/4}$$

Putting the central temperature of the sun $T_{C,\odot} = 1.5 \times 10^7 K$, we get the mass limit for pp chain as:

$$\boxed{M_{min} = 0.1 M_\odot} \tag{3.23}$$

Now, for luminosity, $L \propto M^3$

$$\text{So, } \left(\frac{L_{min}}{L_\odot}\right) = \left(\frac{M_{min}}{M_\odot}\right)^3$$

$$\therefore \boxed{L_{min} = 10^{-3} L_\odot} \tag{3.24}$$

For CNO cycle:

For pp chain, n = 16 and the minimum temperature required $= T_{min} \approx 1.7 \times 10^7 K$
So, $T_C \geq T_{min}$ and $T_C \propto M^{4/19}$
Taking the ratio of minimum temperature and central temperature of the sun and using it with solar mass, we get

$$\frac{M_{min}}{M_\odot} = \left(\frac{T_{min}}{T_{C,\odot}}\right)^{19/4}$$

Putting the central temperature of the sun $T_{C,\odot} = 1.5 \times 10^7 K$, we get the mass limit for the CNO cycle as:

$$\boxed{M_{min} = 1.8 M_\odot} \tag{3.25}$$

Since, for luminosity, $L \propto M^3$

$$\text{So, } \left(\frac{L_{min}}{L_\odot}\right) = \left(\frac{M_{min}}{M_\odot}\right)^3$$

$$\therefore \boxed{L_{min} = 5.832 L_\odot} \tag{3.26}$$

3.3 Modeling with StatStar

StatStar is a simplified stellar structure code designed to numerically model stellar interiors based on the fundamental equations of stellar structure and constitutive relations, as outlined in Section 7. The primary objective of StatStar is to provide a clear and accessible framework for understanding key aspects of numerical stellar astrophysics. To maintain simplicity and stability, the models assume a homogeneous composition, representing zero-age main-sequence (ZAMS) stars.

The code initializes at the outermost layer of the star, progressively integrating inward toward the core. During execution, diagnostic messages are printed to the standard output, particularly upon encountering termination conditions, most of which indicate numerical or physical inconsistencies. The program records the computed stellar model parameters in a text file (starmodl.dat), along with a success or failure indicator. When the simulation proceeds without numerical instabilities, the resulting stellar structure exhibits physically consistent variations in temperature, pressure, and other thermodynamic quantities, transitioning smoothly from the stellar centre to approximately one solar radius.
We run the code using the following inputs:

```
Enter the mass of the star (in solar units): 1
Enter the luminosity of the star (in solar units): 0.860710
Enter the effective temperature of the star (in K): 5500.2
Enter the mass fraction of hydrogen (X): 0.70
Enter the mass fraction of metals (Z): 0.008
```

Figure 3.6: StarStar input parameters used to initialize a stellar model. The specified values represent a star with mass $1M_{\odot}$, luminosity $0.86L_{\odot}$, effective temperature 5500.2 K, and composition defined by X=0.70 (hydrogen) and Z=0.008 (metals).

Our model runs successfully and we get the following output:

```
A Homogeneous Main-Sequence Model
 The surface conditions are:          The central conditions are:
Mtot =  1.000000E+00 Msun             Mc/Mtot    =  4.00418E-04
Rtot =  1.020998E+00 Rsun             Rc/Rtot    =  1.90000E-02
Ltot =  8.607100E-01 Lsun             Lc/Ltot    =  7.67225E-02
Teff =  5.500200E+03 K                Density    =  7.72529E+01
X    =  7.000000E-01                  Temperature =  1.41421E+07
Y    =  2.920000E-01                  Pressure   =  1.46284E+17 dynes/cm**2
Z    =  8.000000E-03                  epsilon    =  3.17232E+02 ergs/s/g
                    dlnP/dlnT   =  2.49808E+00
```

Figure 3.7: The surface and central conditions obtained from the given input data

From the `starmodl.dat` file generated, we plot the following relation:

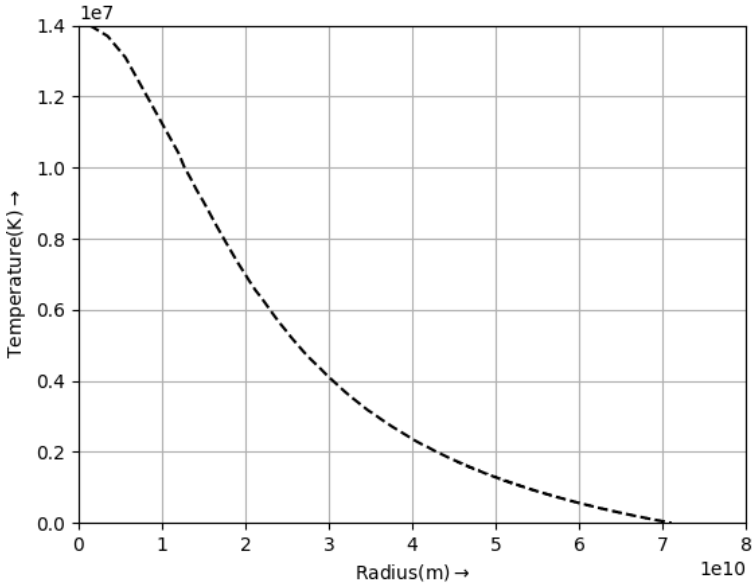

Figure 3.8: Temperature vs radius relation from the generated data of StatStar

The code we have used is available here.

CHAPTER 4

MS Models and Stellar Survey Data

4.1 Stellar Surveys and Data

The study of stellar physics becomes possible only when we can collect information about the stars using the various wavelengths and map them across the sky. Harnessing the power of technology, human beings have created Stellar Surveys that map the positions of stars across the sky. These survey missions are either space-based or ground-based and they collect data on stellar positions, motions, brightness, spectra, and other properties to understand the structure, composition, and evolution of our galaxy and beyond. Stellar surveys can be of the following types:

- Photometric Surveys – Measure the brightness of stars in different wavelengths. For example, SDSS (Sloan Digital Sky Survey), Pan-STARRS
- Spectroscopic Surveys – Obtain detailed spectra of stars. For example, APOGEE (part of SDSS), Gaia RVS
- Astrometric Surveys – Track the precise positions and motions of stars to map the 3D structure of the galaxy. For example: Gaia (by ESA), Hipparcos

Unlike targetted observation of celestial bodies, stellar surveys involve capturing and cataloguing huge sections of the sky at once without the need for complex corrections due to selection biases facilitating statistical analyses. By comparing historical survey data with recent observations, astronomers can detect changes over time—a process that can be automated using advanced image analysis techniques. Before the advent of space-based astrometric missions like Hipparcos and Gaia, several significant efforts were made to compile precise star catalogues:

1. **Henry Draper Catalogue (HD)**: Published between 1918 and 1924, the HD Catalogue provided spectroscopic classifications for 225,300 stars, covering the entire sky down to an apparent photographic magnitude of about 9. It was later expanded by the Henry Draper Extension (HDE) and the Henry Draper Extension Charts (HDEC), bringing the total to 359,083 stars as of August 2017 [27].

2. **Yale Bright Star Catalog**: This catalogue included information on stars brighter than magnitude 6.5, offering detailed data on the most luminous stars visible from Earth [11].

3. **Gliese Catalog of Nearby Stars**: Focusing on stars within 25 parsecs (approximately 82 light-years) of the Sun, this catalogue provided insights into our immediate stellar neighbourhood [15].

To refine stellar positions and distances, ESA launched Hipparcos in 1989. Over .5 years, it measured positions, distances, motions, brightness, and colours of 100,000+ stars, with additional data for over a million more. This mission greatly advanced our understanding of stellar distributions, paving the way for Gaia. In our work, we have mainly looked into Hipparcos, GAIA and SDSS data releases.

4.2 Main Sequence Models and Data

Checking Homologous Model against Data

We now examine data from the **Global Astrometric Interferometer for Astrophysics (GAIA)**, an ESA space telescope launched on December 19, 2013. GAIA surveys nearly two billion objects to create a precise 3D map of the Milky Way. Positioned at the **L2 Lagrange point**, it observes each star about 14 times per year, measuring positions, parallaxes, motions, and brightness variations. GAIA also aids in detecting asteroids, exoplanets, and brown dwarfs. The findings from GAIA Data Release 3 are as follows:

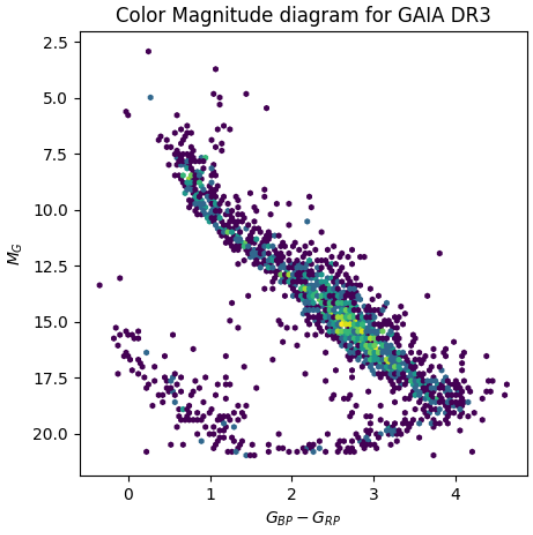

Figure 4.1: The plot displays the Color-Magnitude Diagram (CMD), illustrating the relationship between a star's absolute magnitude and its colour, represented as the difference in magnitude between the G_{BP} and G_{RP} photometric filters. This effectively reflects the star's temperature and spectral type. The data was retrieved using the astroquery module of Python.

Now we shall look into data from the HIPPARCOS catalogue.

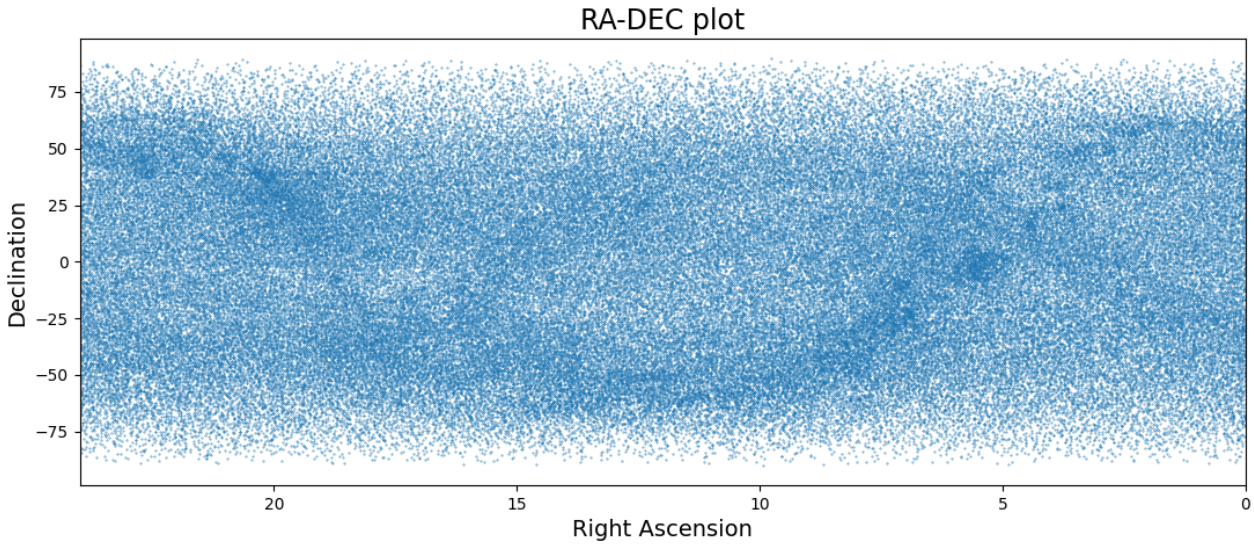

Figure 4.2: Declination vs Right Ascension plot from the HIPPARCOS catalogue

This is the plot for the right ascension versus declination of the stars in the sky, that is their celestial coordinates.

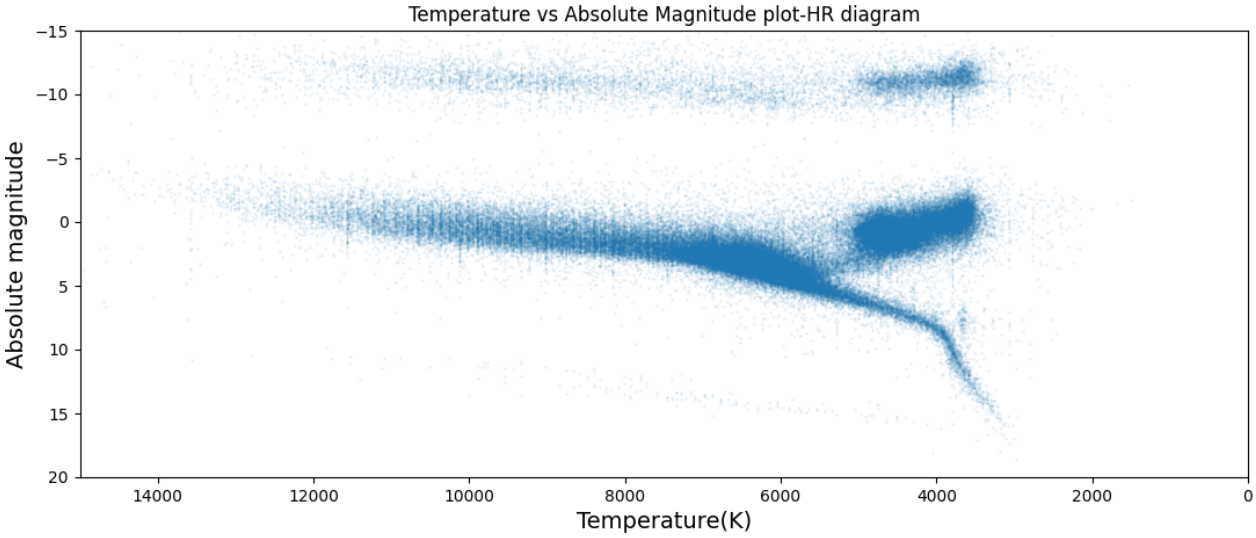

Figure 4.3: H-R diagram from the HIPPARCOS catalogue

The above plot shows the HR diagram- the relation between the absolute magnitude and temperature of about 119614 stars from the HIPPARCOS catalogue. Now let's look into the data of two specific clusters: Aquarius and Virgo.

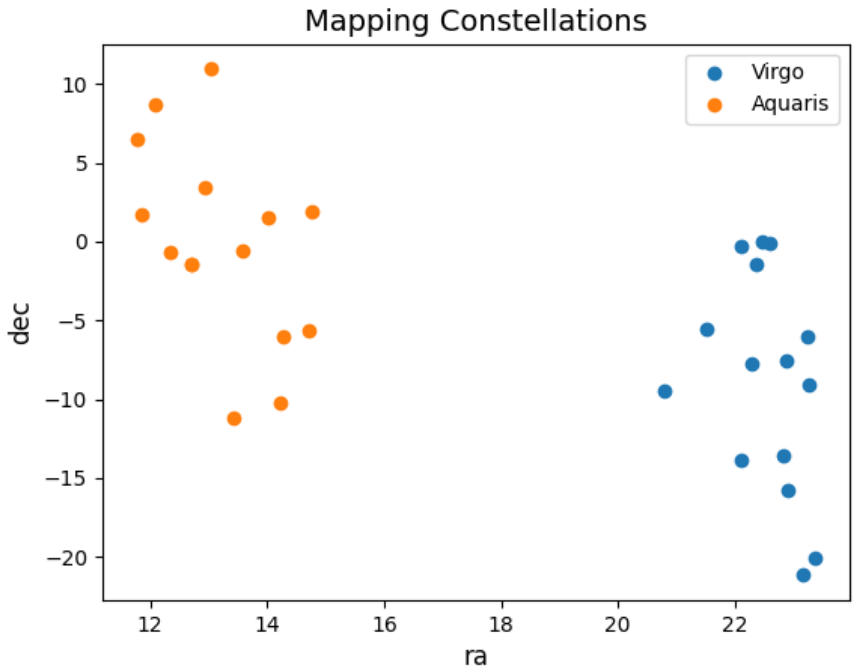

Figure 4.4: Mapping the 15 brightest stars from each of Aquarius and Virgo constellations in an RA Dec plot.

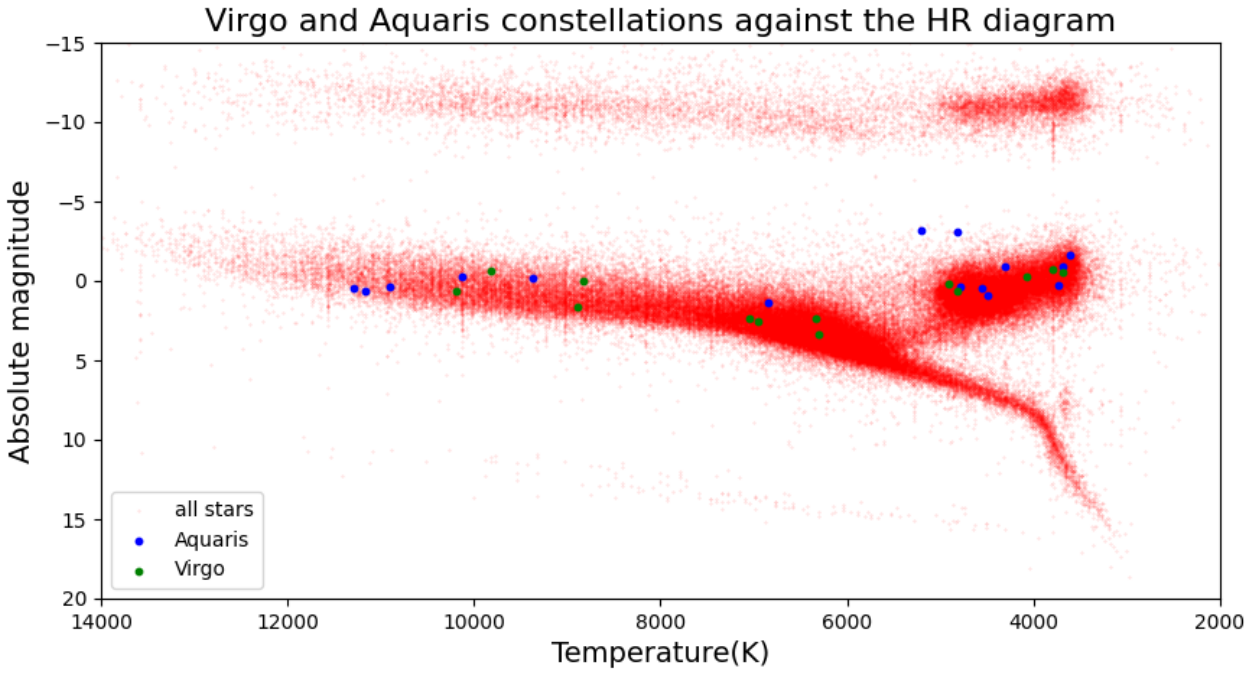

Figure 4.5: Position of the 15 brightest stars from Virgo and Aquarius in the HR Diagram

The top graph i.e. Figure 4.4 shows what the constellation Virgo and Aquaris looks like in the sky. The lower plot shows those same stars (as red points) on the same absolute magnitude vs. temperature graph in Figure 4.3.

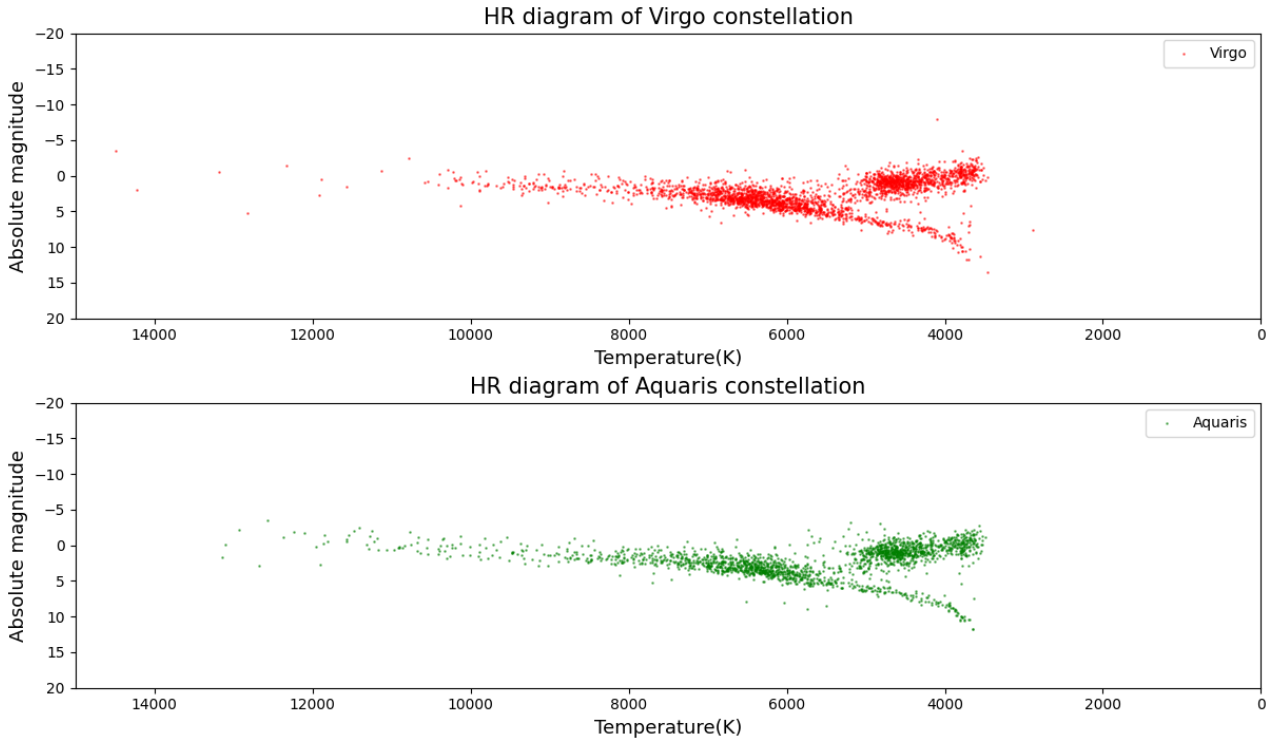

Figure 4.6: HR diagram of the stars in Virgo cluster (top), Aquaris cluster (bottom)

The above figure shows the HR diagram of the Virgo and Aquaris clusters, indicating the number of stars going through the pp chain, the CNO cycle and also the main sequence turnoff for each.

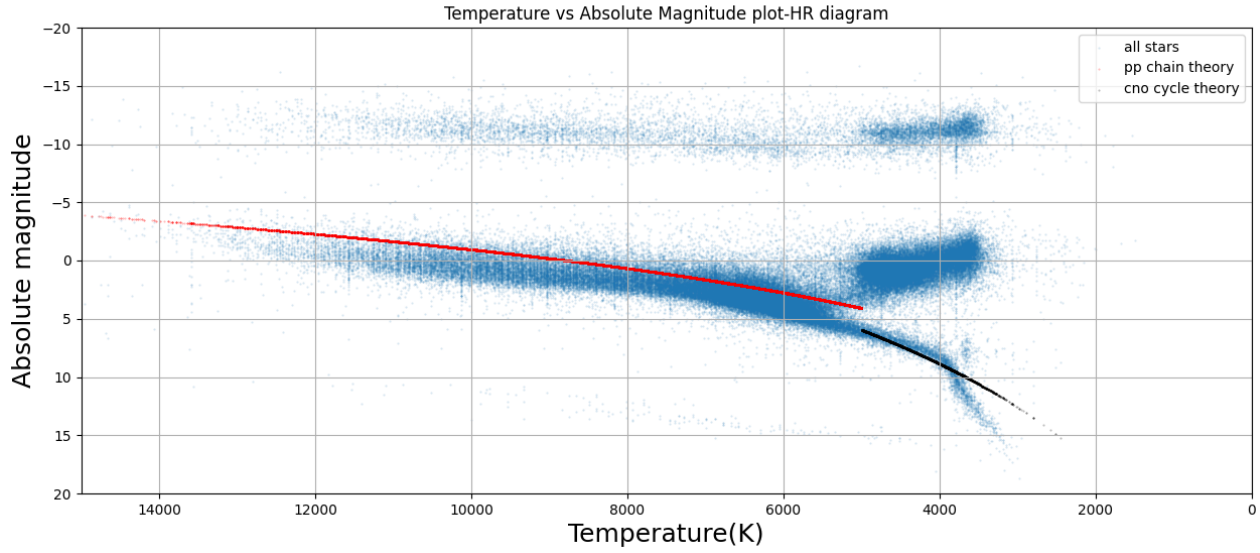

Figure 4.7: HR diagram comparing pp chain and CNO cycle models with HIPPARCOS data.

In Figure 4.7, we fit homologous models of the pp chain and CNO cycle during the main sequence phase to HIPPARCOS data. The pp chain fits well, while the CNO cycle matches accurately above 2000 K up to the turnoff.

Isochrone Fitting of Cluster Data

Stellar Clusters are groups of stars that have formed together from the same molecular cloud and are bound by mutual gravitational attraction. These clusters provide valuable insights into stellar formation and evolution, as their stars share similar ages and compositions. They are basically two types:

1. Open clusters: They are loosely bound young clusters and often disperse due to gravitational interaction with other celestial bodies. For example, the Pleiades and Beehive Cluster.

2. Globular Clusters: They are strongly bound spherical clusters and are usually older, found in halos of galaxies. For example, Messier 2 (NGC 7089) and Messier 13 (NGC 6205)

We shall try to fit an isochrone in the SDSS stellar data for the M2 Cluster. In astronomy, an isochrone is a curve plotted on the HR diagram that connects points representing stars of the same age but varying masses. Isochrones are particularly valuable for studying star clusters because it's reasonable to assume that all member stars formed simultaneously from the same molecular cloud. By comparing observed data with isochrones, astronomers can infer not only the age but also other properties of the cluster, such as its distance and chemical composition.

Our aim is to find the best-fit isochrone for the M2 stellar cluster varying the following parameters one by one: Age, Metallicity, and Distance. Extracting data from the SDSS survey, we initially fixed the metallicity [Fe/H]= -1.65 and distance= 13 kpc. Varying the age as 12 Gyrs, 13 Gyrs and 14 Gyrs, we get the following:

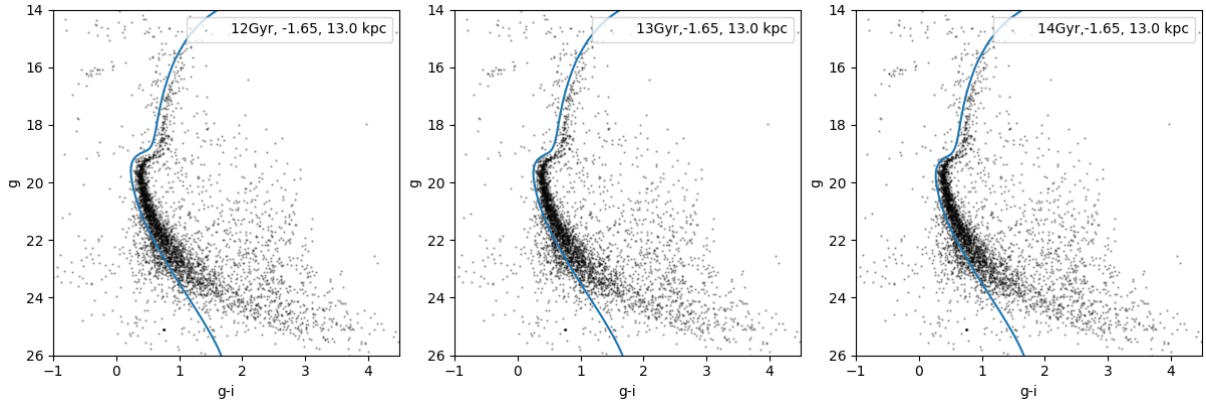

Figure 4.8: Color-Magnitude Diagram (CMD) showing multiple MIST isochrones with variation of age, and metallicity and distance fixed at arbitrary values; Age = 14 Gyr shows the best fit; The black scattered points represent the SDSS data, the blue plot is the isochrone.

Thus the isochrone with an age of 14 Gyrs has the best fit. Fixing this age, we shall now generate and use isochrones with varying metallicity: -1.55, -1.60, -1.65, -1.75. Fitting to the data:

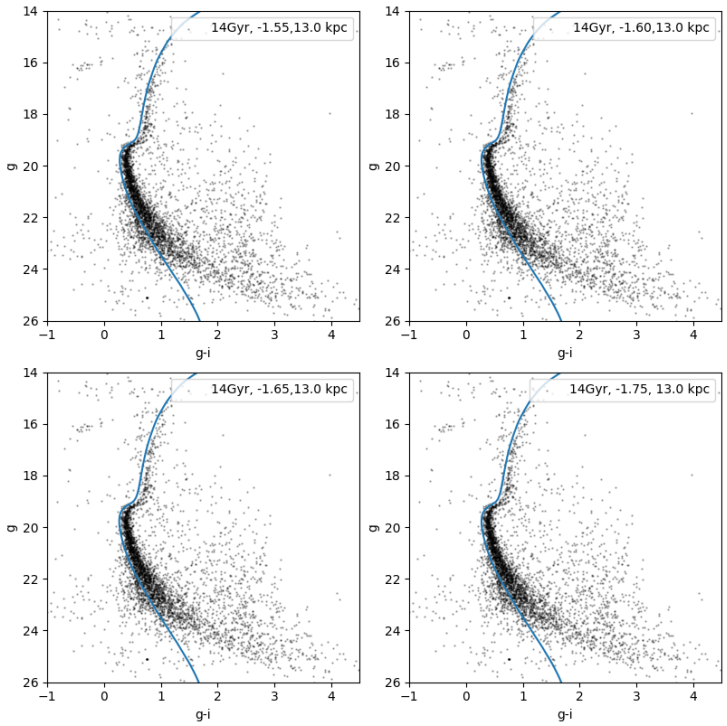

Figure 4.9: CMD illustrating the variation of MIST isochrones with different metallicities while keeping age and distance fixed; Metallicity [Fe/H]= -1.55 shows the best fit.

Metallicity = -1.55 and Age = 14 Gyrs show the best fit so far. So keeping these two parameters constant, we vary the distance from 12 kpc to 15 kpc in steps of 0.5 kpc, as follows:

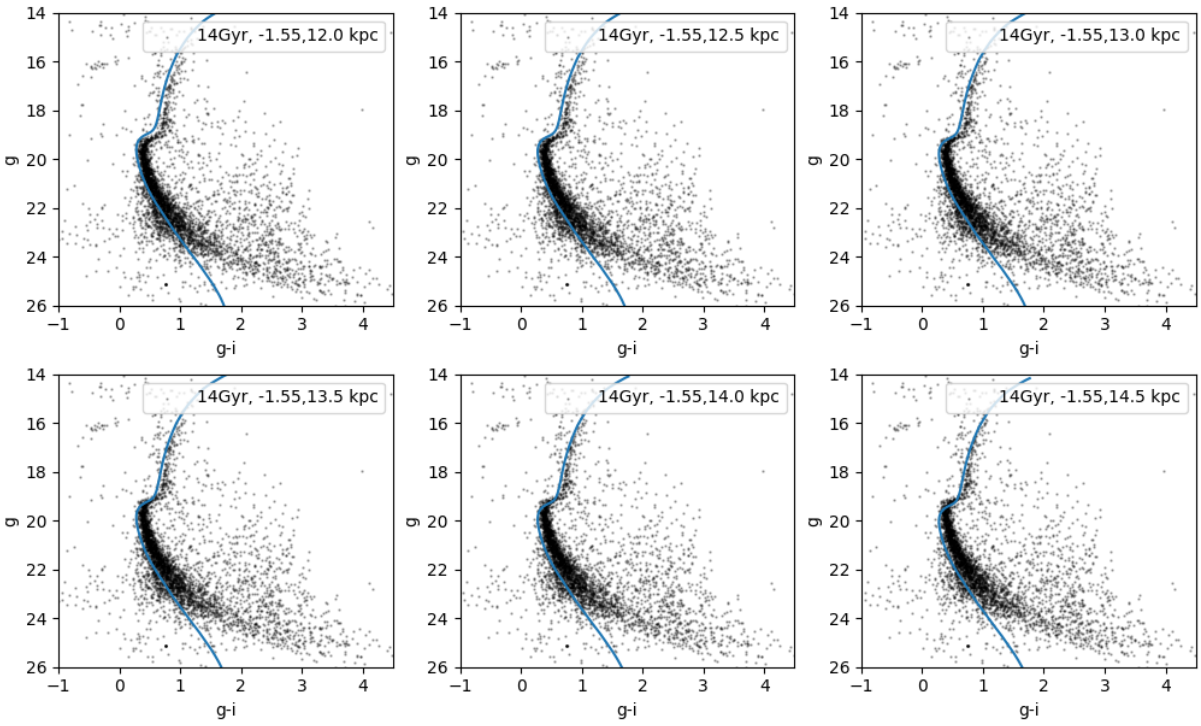

Figure 4.10: CMD showing MIST isochrones at varying distances with fixed [Fe/H] = -1.55 and age = 14 Gyr. The best fit occurs at 13.5 kpc, aligning closely with the observed stellar distribution.

Thus with iterations of each of the three parameters we find that **Messier 2** cluster : (i) is **14 Gigayears** old, (ii) has a metallicity [Fe/H] of **-1.55**, (iii) at a distance of approx **13.5 kpc** from earth.

Now, to improve the accuracy of isochrone fitting and reduce contamination from field stars, we defined a closed polygonal selection region encompassing the main sequence, turn-off, and evolved stars while excluding clear outliers in the Color-Magnitude Diagram (CMD). The selection criteria are based on the expected distribution of cluster members within the CMD, considering observational uncertainties and potential photometric errors.

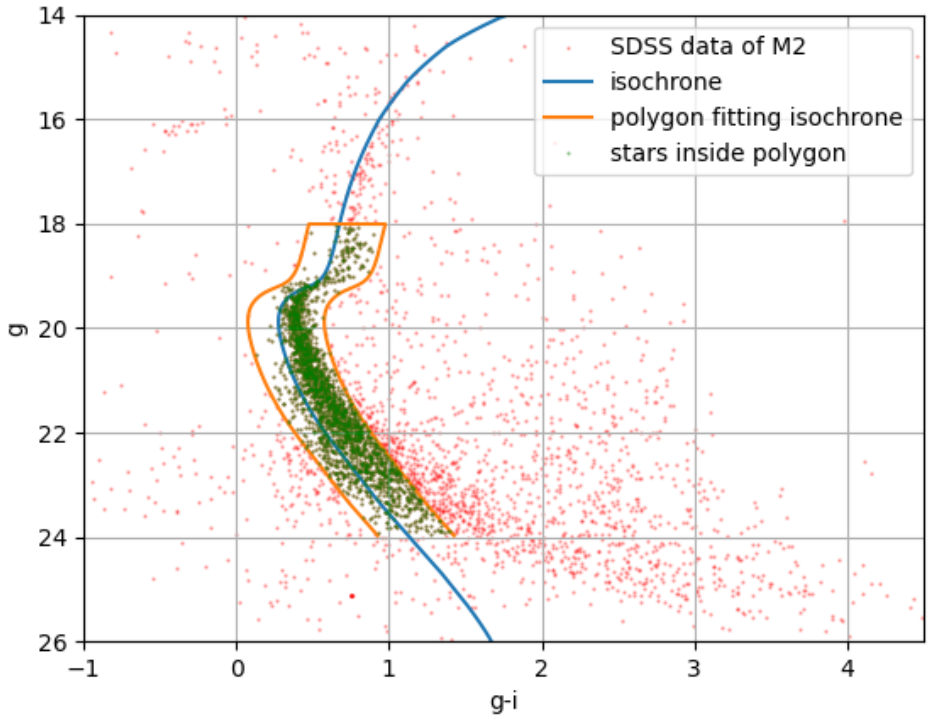

Figure 4.11: Color-Magnitude Diagram (CMD) with the selected MIST isochrone enclosed within a polygonal region. The polygon marks the boundary used to filter stars that closely follow the isochrone, minimizing contamination from field stars and improving the accuracy of the fit. The selected stars within this region were used for further parameter estimation, refining age and metallicity determinations.

The code we have used is here: Isochrone Fitting Notebook

CHAPTER 5

Post Main Sequence Evolution

5.1 Nucleosynthesis in Post Main Sequence phase

In the first few minutes following the Big Bang, nucleosynthesis produced primarily hydrogen (${}^1_1H$ and ${}^2_1H$) and helium (${}^3_2He$ and ${}^4_2He$), along with a minuscule amount of lithium (${}^7_3Li$). However, heavier isotopes were not significantly formed. As a result, the early universe was composed mostly of hydrogen (76% by mass) and helium (24% by mass).
Within stars, hydrogen burning converts protons into helium nuclei but does not generate heavier elements. The CNO cycle, for example, increases nitrogen abundance at the cost of carbon, as ${}^{12}_6C$ transforms into ${}^{14}_7N$. The formation of elements beyond helium—termed metals in astronomy—occurs through stellar nucleosynthesis processes that extend beyond hydrogen burning.
Primordial nucleosynthesis of heavier elements is prevented by:

1. Greater Coulomb barrier of elements with higher atomic number.
2. Lack of stable isotopes between mass numbers 5 and 8.
3. Decreasing density of matter due to expansion of the universe.

So, although nucleosynthesis in the Big Bang produced the raw materials from which the first stars formed, stellar evolution has further enriched the interstellar medium with elements heavier than hydrogen and helium [3]. From stellar nucleosynthesis, we see:

1. H and He has almost 1000 the abundance of any other element.
2. Due to the lack of stable isotopes, elements with atomic numbers 3, 4, and 5 are virtually absent.
3. Carbon (C), oxygen (O), neon (Ne) and silicon (Si) have a relatively large abundance.
4. Elements heavier than iron (Fe) are less abundant and are produced by neutron capture in later evolutionary stages of stars.

Triple alpha process

In stars with mass greater than $0.5M_{\odot}$, the core becomes hot and dense for He-burning with $T_C \sim (1-2) \times 10^8 K$ and $\rho_C \sim (10^5 - 10^8) kg/m^3$. There are three main steps in He burning:

Step 1 : ${}^4_2He + {}^4_2He \leftrightarrow {}^8_4Be$
Step 2 : ${}^4_2He + {}^8_4Be \leftrightarrow {}^{12}_6C^*$
Step 3 : ${}^{12}_6C^* \rightarrow {}^{12}_6C + 2\gamma$

Though apparently simple, there are lots of intricacies in the steps, such as stable mass gaps at A=5 and A=8 that have to be bypassed.

Step 1:

${}^8_4Be$ is an unstable nucleus. In fact, all mass 8 nuclei are unstable. The reaction is endothermic and the beryllium-8 nucleus has an energy of only 91.8 keV greater than the two α particles. The ground state has a width of 2.5 eV, so the lifetime $\tau \approx \frac{\hbar}{\Delta E} = 2.6 \times 10^{-16} s$. So ${}^8_4Be$ does decay back to two α particles. Now the time taken by thermal α particles to move a distance equal to its diameter is less than $10^{-20} s$. So if there would have been no resonance in the ground state of 8-beryllium, the two α particles would have remained 'stuck' for less than $10^{-20} s$. Now the 8-beryllium stays stuck for $\sim 10^{-16} s$ and in that duration, another thermal α particle (the third α particle) combines radiatively with it [9].

Step 2:

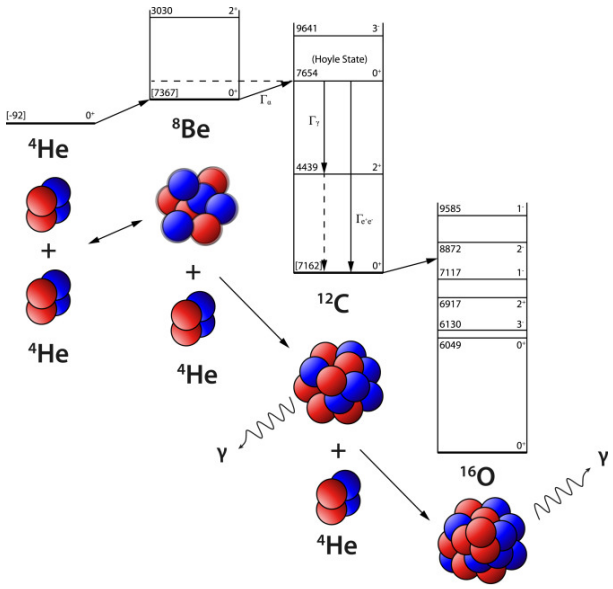

Figure 5.1: Energy Levels of He Burning Nuclei [9]

The α capture by ${}^8_4Be$ is possible because of its tiny equilibrium abundance.There is again an energy gap of 287.7 keV. As predicted by Hoyle and later experimentally established by Fowler, there is an energy level of ${}^{12}C$, the 7.65 MeV O+ state of ${}^{12}C$. This is the Hoyle level; he

predicted that the overall reaction will not be fast enough if the $^8Be(\alpha,\gamma)^{12}C$ reaction is not resonant [9].

Step 3:

Around 1 in 2500 nuclei of $^{12}C^*$ gives ^{12}C and γ, the rest break back to ^8Be and γ.

Further He burning

$$^4_2He + ^{12}_6C \rightarrow ^{16}_8O + \gamma$$

This is one of the most interesting reactions of stellar nucleosynthesis, as it determines how much carbon-12 produced in the triple α process changes to oxygen-16. $^{12}C(\alpha,\gamma)^{16}O$ in the He core of a star takes place simultaneously with the triple α process. The C/O ratio greatly influences the star's future evolution. It determines the luminosity of runaway thermonuclear burning in the white dwarfs involved in type Ia supernovas.
Now this reaction is interesting in the sense that its rate and S factor are not known and is one of the long-standing problems in nuclear astrophysics. If the reaction rate was too low, the conversion of C to O would be inefficient and the abundance of oxygen and other heavier elements would be observed. If the reaction were too rapid, the net helium burn would be $4\alpha \rightarrow {}^{16}O$. The reaction $^{12}C(\alpha,\gamma)^{16}O$ would seem to be non-resonant in that no state in ^{16}O lie near E_0 plus the mass of ^{12}C and ^4He. The $^{12}C + {}^4He$ state lies at 7.161 MeV. Below this, at 7.115 MeV, there is a 1^- state with a Gamow width of only $\Gamma_\alpha = 0.060\,eV$. But the state has a finite lifetime against radiative de-excitation and therefore a corresponding indeterminacy in its energy. It is thought that $^{12}C(\alpha,\gamma)^{16}O$ can occur through the tails of this state, but the rate has been difficult to measure. The 7.162 MeV 0^+ level of carbon-12 and 7.115 MeV 1^- level of oxygen-16 are so close that it becomes difficult to separate those [3], [9], [28].

Measurement of Reaction Rates

The $^{12}C(\alpha,\gamma)^{16}O$ in He burning takes place around CoM energies of 300 keV. Direct measurements cannot determine its reaction rate since the cross section is very small ($\approx 10^{-17}$ barns). The extrapolation to low energies is also difficult as the cross-section of this energy region is a mixture of the ground state and cascade transitions with no state of natural parity in ^{16}O available for radiative capture near 300 keV energy. [28]

Theoretically, we have tried model as well as phenomenological approaches to extrapolation at low energies. Some key methods have been:

1. R-Matrix analysis of spectrum of delayed α particles (F.C. Baker, 1971).
2. Scattering cross-section method (P. Tischhauser et al., 2009).
3. Inverse kinematics (K.U. Kettner et al., 1982).
4. Alpha transfer to determine model-independent ANC (C.R. Brune et al., 1999).

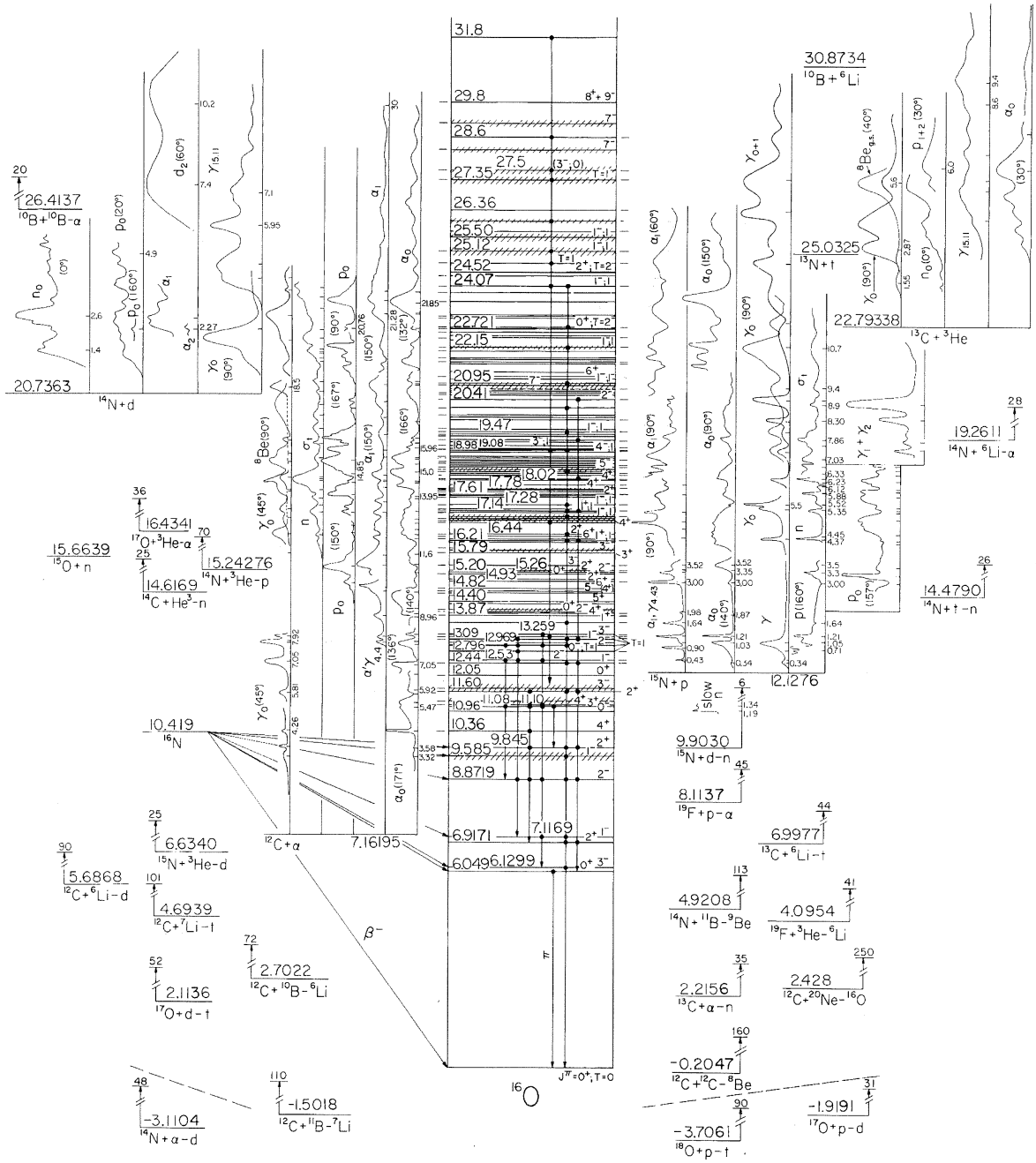

Figure 5.2: Energy Levels of Oxygen-16

5.2 Study of ^{16}O Resonance using R-Matrix Framework

The R-Matrix Framework

The R-Matrix theory, developed by Wigner and Eisenbud (1947), is a powerful mathematical framework for describing resonances in nuclear reactions. It provides a systematic way to analyze quantum mechanical scattering processes, effectively handling the boundary conditions between the internal nuclear interaction region and the external Coulomb region. This approach is particularly useful when dealing with low-energy reactions where direct measurements are challenging due to extremely small cross sections.

The R-matrix is defined at a channel radius a that separates the nuclear interior and the asymptotic region [23]:

$$R_{cc'}(E) = \sum_{\lambda} \frac{\gamma_{c\lambda}\gamma_{c'\lambda}}{E_\lambda - E}$$

where:

- E_λ = Eigen Energy of the resonance state λ
- $\gamma_{c\lambda}$ = Reduced width amplitude for channel c
- E = Center-of-mass energy
- $R_{cc'}(E)$ = R-matrix element for channels c and c'

The reaction cross-section is related to the R-matrix via the scattering matrix S:

$$S_{cc'} = e^{2i\delta_c}(\delta_{cc'} - 2iP_cR_{cc'}(E))$$

where P_c is the penetrability factor and δ_c is the phase shift.

Fitting Cross Section of Elastic Scattering $^{12}C(\alpha,\alpha)^{12}C$ using AZURE2

AZURE2 is an R-matrix code written in C++. Its purpose is the calculation of differential and total cross-sections of interest in nuclear astrophysics. The R-matrix sections of the code follow the formulation of A.M.Lane and R.G.Thomas (LT) [23]. The code for the R-matrix cross-section calculations is embedded in a MINUIT (CERN) least squares batch mode environment so that the theoretical calculations can be fitted to the experimental data. [24]

We shall use this code to look into the reaction $^{12}C(\alpha,\alpha)^{12}C$, where ^{16}O forms the excited energy level. We have analysed the resonances of ^{16}O by fitting the experimental data using AZURE2. The data used is taken from the IBANDL website, Bogdanovic-Radovic data set [20].
Inputs required for particle information:

- For lighter particle, $J = 0^+$, Z=2 and M=4

- For heavier particle, $J = 0^+$, Z=6 and M=12
- Excitation energy = 0 MeV
- Separation Energy = 7.167 MeV
- Channel Radius = 5.5 fm

The data segments are differential, in the energy range 1.8-4.9 MeV across five lab angles in degrees: 30, 45, 60, 135 and 150. Adding compound energy levels (detailed steps in [25]), we run the calculations and fit the data. The best fit for two segments of data is as follows:

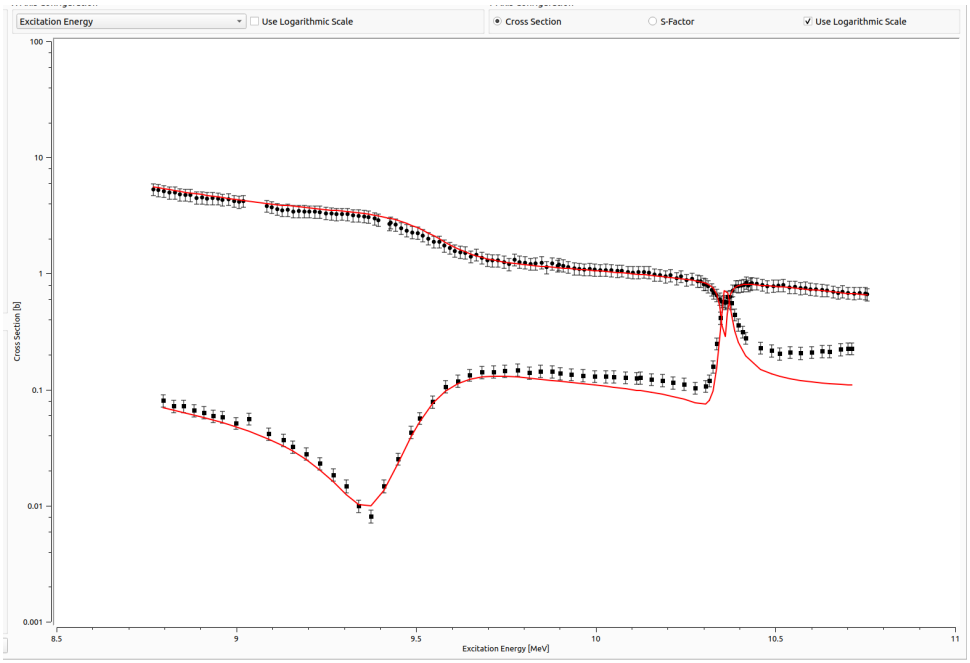

Figure 5.3: R-Matrix analysis, showing final fit for two segments of data, for cross section and CoM energy

From the plot, we understand that ^{16}O nucleus has resonant energy levels at 1^- corresponds to 9.5 MeV and 4^+ corresponds to 10.4 MeV. Consulting literature (or TUNL [26]), we see that 1^- corresponds to 9.580 MeV and 4^+ corresponds to 10.35 MeV. These are the known resonance levels and will improve the fit.

In nuclear physics, a resonance occurs when the energy of the interacting particles matches an excited energy state of the resulting nucleus. This matching increases the reaction cross-section, thereby elevating the likelihood of the fusion process. The existence of specific resonant energy levels in ^{16}O enhances the fusion probability in the $^{12}C(\alpha,\gamma)^{16}O$. reaction by increasing the reaction cross-section at energies corresponding to these states. This enhancement is crucial for stellar helium burning and influences the synthesis of elements in the universe [9]

CHAPTER 6

Conclusion

After a star finishes its time in the Post Main Sequence phase, it moves to the next phase depending on its mass. For low and intermediate-mass stars, the final stage is usually a white dwarf or a planetary nebula. For more massive stars, either a Type II supernova explosion occurs or it becomes a neutron star. Stars with mass greater than $3M_{\odot}$ become black holes.

In conclusion, we have looked at the internal structure of stars and tried to understand their evolution both from the point of view of nucleosynthesis as well as homologous modelling through stellar structure equations. We have modelled Main Sequence stars using this theoretical homologous model as well as through a pipeline called StatStar. The HR diagram and CMD have been used from surveys like GAIA and HIPPARCOS to compare theoretical models with data. We also looked into the MIST code to generate isochrones for NGC 7089 and find the best fit for SDSS data. In the Post Main Sequence Phase, we calculated the relation between cross section and CoM energy for the $^{12}C(\alpha,\alpha)^{12}C$ reaction and looked into the resonant energy levels of ^{16}O.

In future, we plan to look into more evolutionary codes like Modules for Experiments in Stellar Astrophysics (MESA) [29] and a radiation hydrodynamics code STELLA and compare the results. We shall also generalise the cluster fitting algorithm in Python through the use of relevant packages. Further research in this field with the use of evolving technologies like ML and AI, along with advancements in instrumentation for recreating nuclear reactions of astrophysical environments with better precision shall answer a lot of open questions like the origin of Stellar IMF, the Lithium abundance anomaly in low mass stars and so on.

APPENDIX *A*

CMD using GAIA DR3

To generate the plot in 4.1 from GAIA DR3 using Python

```
import numpy as np
import pandas as pd
import matplotlib.pyplot as plt
from astroquery.gaia import Gaia
from astropy.table import table
from matplotlib import colors

tables=Gaia.load_tables(only_names=True)
# external.gaiaedr3_gcns_main_1
query1 = """SELECT
    source_id, ra, dec, phot_g_mean_mag, phot_bp_mean_mag,
   phot_rp_mean_mag, parallax
    FROM external.gaiaedr3_gcns_main_1"""
job=Gaia.launch_job(query1)
results=job.get_results()

color=results["phot_bp_mean_mag"] -results["phot_rp_mean_mag"]
fig, ax= plt.subplots(figsize=(5,5))

ax.hexbin(color,results["phot_g_mean_mag"],bins='log',mincnt=1)
ax.invert_yaxis()
ax.set_xlabel("Color")
ax.set_ylabel("G")
ax.set_title("Color mag diagram")
plt.show()
```

APPENDIX *B*

From the HIPPARCOS catalogue

Importing data for star catalogue analysis

```
import numpy as np
import pandas as pd
import matplotlib.pyplot as plt

data=pd.read_csv(r"stars.csv")
```

Declination vs Right Ascension plot (4.2) for each star in the data table

```
fig=plt.figure(figsize=(13,5))
plt.scatter(data["ra"], data["dec"], s=0.1)
plt.xlabel("Right Ascension",fontsize=14)
plt.ylabel("Declination",fontsize=14)
plt.title("RA-DEC plot", fontsize=17)
plt.xlim(24,0)
```

Absolute Magnitude vs Temperature plot (4.3) for each star in the data table

```
fig,ax=plt.subplots(figsize=(13,5))
ax.set_ylim([20,-15])
ax.set_xlim([0,15000])
ax.invert_xaxis()
ax.scatter(data["temp"], data["absmag"], s=0.1, alpha=0.2)
ax.set_xlabel("Temperature(K)",fontsize=14)
ax.set_ylabel("Absolute magnitude",fontsize=14)
ax.set_title("Temperature vs Absolute Magnitude plot-HR diagram")
```

APPENDIX *C*

Aquaris and Virgo from HIPPARCOS

Importing data for star catalogue analysis

```
import numpy as np
import pandas as pd
import matplotlib.pyplot as plt

data=pd.read_csv(r"stars.csv")
```

Mapping Aquaris and Virgo in RA-DEC (4.4)

```
Aquaris=data.query('con=="Aqr"')
star=Aquaris.sort_values("mag").head(15)
Virgo=data.query('con=="Vir"')
con=Virgo.sort_values("mag").head(15)
plt.scatter(star["ra"], star["dec"],label="Virgo")
plt.scatter(con["ra"], con["dec"],label="Aquaris")
plt.xlabel("ra",fontsize=12)
plt.ylabel("dec",fontsize=12)
plt.title("Mapping Constellations",fontsize=14)
plt.legend()
```

Plotting 15 stars from Aquaris and Virgo each against the HR diagram of all stars in the catalog (4.5)

```
fig,ax=plt.subplots(figsize=(10,5))
ax.set_ylim([20,-15])
ax.set_xlim([2000,14000])
```

```
ax.invert_xaxis()
ax.scatter(data["temp"], data["absmag"], s=0.1,
    alpha=0.2,color="red",label="all stars")
ax.set_xlabel("Temperature(K)",fontsize=14)
ax.set_ylabel("Absolute magnitude",fontsize=14)
ax.scatter(star["temp"], star["absmag"], s=10,color='blue',
    label="Aquaris")
ax.scatter(con["temp"], con["absmag"],
    s=10,color='green',label="Virgo")
ax.set_title("Virgo and Aquaris constellations against the HR
    diagram", fontsize=16)
ax.legend()
```

HR diagram plot of all stars from the Aquaris and Virgo cluster (4.6)

```
# sorting the data to plot
virgo_data=data.query('con=="Vir" and absmag>=-8')
aqua_data=data.query('con=="Aqr" and absmag>=-8')
T_vir=virgo_data["temp"]
M_vir=virgo_data["absmag"]
T_aqua=aqua_data["temp"]
M_aqua=aqua_data["absmag"]

# plotting separately
fig,ax=plt.subplots(2,1,constrained_layout=True,figsize=(12,7))
ax[0].set_ylim([20,-20])
ax[0].set_xlim([0,15000])
ax[0].invert_xaxis()
ax[0].scatter(virgo_data["temp"],virgo_data["absmag"],color='red',s=0.8,
    alpha=0.5,label="Virgo")
ax[0].set_xlabel("Temperature(K)",fontsize=13)
ax[0].set_ylabel("Absolute magnitude",fontsize=13)
ax[0].set_title("HR diagram of Virgo constellation",fontsize=15)
ax[0].legend()
ax[1].set_ylim([20,-20])
ax[1].set_xlim([0,15000])
ax[1].invert_xaxis()
ax[1].scatter(aqua_data["temp"],aqua_data["absmag"],color='green',s=0.8,
    alpha=0.5, label="Aquaris")
ax[1].set_xlabel("Temperature(K)",fontsize=13)
ax[1].set_ylabel("Absolute magnitude",fontsize=13)
ax[1].set_title("HR diagram of Aquaris constellation",fontsize=15)
ax[1].legend()
```

APPENDIX *D*

Fitting MS Model with HIPPARCOS Data

Importing data for star catalogue analysis

```
import numpy as np
import pandas as pd
import matplotlib.pyplot as plt

data=pd.read_csv(r"stars.csv")
```

Fitting the equations of pp chain and CNO cycle with the stellar data table

```
# pp chain
# Include stars with temperatures greater than 5000 K
pp_data=data.query('temp>5000')
T_pp=pp_data["temp"]
M_pp=pp_data["absmag"]
# Define constants for luminosity calculation
L0=3.828e+26
M0=4.83
L_pp=L0*10**((M0-M_pp)/2.5)

def pp(T_pp,n1,a1):  # Define the pp chain fitting function
 return((12*(n1+3)/(n1+7))*np.log(T_pp)+(a1*3*(n1+3)/(n1+7)))
bounds = ([3.9, -np.inf], [4.5, np.inf])
parameters1, covariance1 = curve_fit(pp, T_pp,
   np.log(L_pp),bounds=bounds)

n1=parameters1[0]
a1=parameters1[1]
```

```
# Fitted luminosity and absolute magnitudes from pp chain model
log_L_pp=pp(T_pp,n1,a1)
L_pp=np.exp(log_L_pp)
M_pp=M0-2.5*np.log10(L_pp/L0)


# CNO cycle
# Include stars with temperatures <= 5000 K and abs mag >= 5
cno_data=data.query('temp<=5000 and absmag>=5')
T_cno=cno_data["temp"]
M_cno=cno_data["absmag"]
# Define constants for luminosity calculation
L0=3.828e+26
M0=4.83
L_cno=L0*10**((M0-M_cno)/2.5)

def cno(T_cno,n2,a2):  # Define the CNO cycle fitting function
 return((12*(n2+3)/(n2+7))*np.log10(T_cno)+(a2*3*(n2+3)/(n2+7)))
bounds = ([15, -np.inf], [16.5, np.inf])
parameters2, covariance2 = curve_fit(cno, T_cno,
    np.log10(L_cno),maxfev=10000,bounds=bounds)

n2=parameters2[0]
a2=parameters2[1]
# Fitted luminosity and absolute magnitudes from CNO cycle model
log_L_cno=cno(T_cno,n2,a2)
L_cno=10**(log_L_cno)
M_cno=4.83-2.5*np.log10(L_cno/3.828e+26)


# plotting against HR
fig,ax=plt.subplots(figsize=(15,6))
ax.set_ylim([20,-20])
ax.set_xlim([0,15000])
ax.invert_xaxis()
ax.scatter(data["temp"], data["absmag"], s=0.2, alpha=0.2, label="all
    stars")  # for all stars
ax.scatter(T_pp,M_pp,color='red', s=0.2, alpha=0.3,label="pp chain
    theory")  # for pp chain stars
ax.scatter(T_cno,M_cno,color='black',s=0.2, alpha=0.3, label="cno
    cycle theory")  # for CNO cycle stars
ax.legend()
ax.set_xlabel("Temperature(K)",fontsize=13)
ax.set_ylabel("Absolute magnitude",fontsize=13)
ax.set_title("Temperature vs Absolute Magnitude plot-HR
    diagram",fontsize=16)
plt.grid()
```

APPENDIX *E*

R-Matrix Configuration

Data Segments

```
<segmentsData>
1   1   1   1.8   4.9   30   30   1   1   0   0
/home/sanchari/c-12-new.dat
1   1   1   1.8   4.9   45   45   1   1   0   0
/home/sanchari/c-12-new.dat
1   1   1   1.8   4.9   60   60   1   1   0   0
/home/sanchari/c-12-new.dat
1   1   1   1.8   4.9   135   135   1   1   0   0
/home/sanchari/c-12-new.dat
1   1   1   1.8   4.9   150   150   1   1   0   0
/home/sanchari/c-12-new.dat
</segmentsData>
```

Parameters for Compound Nucleus Levels from the `parameters.out` file

PHYSICAL LEVEL PARAMETERS (BOUNDARY CONDITION SET TO SHIFT AT E_LEVEL)

```
J = 0.0+ E_level = 15.0000 MeV ITERATIONS = 0
R = 1 l = 0 s = 0.0 G = 0.000000 meV   g_int = 0.000000 MeV(1/2)
g_ext = (0.000000,0.000000) MeV(1/2)
J = 1.0- E_level = 9.5850 MeV ITERATIONS = 0
R = 1 l = 1 s = 0.0 G = 420.000000 keV   g_int = 0.781650 MeV(1/2)
g_ext = (0.000000,0.000000) MeV(1/2)
J = 2.0+ E_level = 15.0000 MeV ITERATIONS = 0
```

```
R = 1 l = 2 s = 0.0 G = 0.000000 meV   g_int = 0.000000 MeV^(1/2)
g_ext = (0.000000,0.000000) MeV^(1/2)
J = 3.0^- E_level = 15.0000 MeV ITERATIONS = 0
R = 1 l = 3 s = 0.0 G = 0.000000 meV   g_int = 0.000000 MeV^(1/2)
g_ext = (0.000000,0.000000) MeV^(1/2)
J = 4.0^+ E_level = 10.3560 MeV ITERATIONS = 0
R = 1 l = 4 s = 0.0 G = 26.000000 keV   g_int = 0.443824 MeV^(1/2)
g_ext = (0.000000,0.000000) MeV^(1/2)
```

Bibliography

[1] Carroll, B. W., Ostlie, D. A. *An Introduction to Modern Astrophysics*. Second Edition, Addison Wesley.

[2] Prialnik, D. *An Introduction to the Theory of Stellar Structure and Evolution*. Second Edition, Cambridge University Press.

[3] Ryan, S. G., Norton, A. J. *Stellar Evolution and Nucleosynthesis*. Cambridge University Press (2010)

[4] Fatima1, H., Mushtaq, M., Faisal Ur Rahman, S. *Age Estimates of Universe: from Globular Clusters to Cosmological Models and Probes*. Journal of GeoSpace Science, ISSN:2413-6093 (2016)

[5] *Pulsating Variable Stars and the Hertzsprung-Russell (H-R) Diagram*. CHANDRA X-RAY OBSERVATORY; Accessed on 26th March 2025, from https://chandra.harvard.edu/edu/formal/variable_stars/bg_info.html

[6] Gotame R.C. (Nov 8, 2020). *Harvard Spectral Classification*. Physics Feed; Accessed on 26th March 2025, from https://physicsfeed.com/post/harvard-spectral-classification/

[7] *Main Sequence*. Wikipedia; Accessed on 26th March 2025, from https://en.m.wikipedia.org/wiki/Main_sequence

[8] *The Mysteries of the Physical World*. Libraries, Michigan State University; Accessed on 26th March 2025, from https://openbooks.lib.msu.edu/collegephysics/chapter/tunneling/

[9] David Arnett. *Supernovae AND Nucleosynthesis*. Princeton University Press (1996)

[10] *Gaia Factsheet*. The European Space Agnency; Accessed on 30th March 2025, from https://www.esa.int/Science_Exploration/Space_Science/Gaia/Gaia_factsheet

[11] *Yale Bright Star Catalog*. NASA Goddard Space Flight Center; Accessed on 30th March 2025, from http://tdc-www.harvard.edu/catalogs/bsc5.html

[12] *Stellar Data Repository*; Accessed on 30th March 2025, from https://github.com/adamlamee/CODINGinK12/blob/master/data/stars.csv

[13] *SDSS Data Release 16.* Accessed on 30th March 2025, from https://www.sdss4.org/dr16/

[14] *GAIA Data Release 3.* European Space Agency; Accessed on 30th March 2025, from https://www.cosmos.esa.int/web/gaia/dr3

[15] *CNS3 - Gliese Catalog of Nearby Stars, 3rd Edition.* NASA Goddard Space Flight Center; Accessed on 30th March 2025, from https://heasarc.gsfc.nasa.gov/W3Browse/star-catalog/cns3.html

[16] *William Herschel- Astronomy, Stars, Evolution.* Britannica; Accessed on 31st March 2025, from https://www.britannica.com/biography/William-Herschel

[17] Helge Kragh. *Reluctant Pioneer of Nuclear Astrophysics: Eddington and the Problem of Stellar Energy.*

[18] EDDINGTON, A. S. *The Internal Constitution of the Stars.* Nature 106, 14–20 (1920). https://doi.org/10.1038/106014a0

[19] Wiescher, M. *The History and Impact of the CNO Cycles in Nuclear Astrophysics.* Phys. Perspect. 20, 124–158 (2018). https://doi.org/10.1007/s00016-018-0216-0

[20] *IBDANL*, Nuclear reaction data repository https://nds.iaea.org/exfor/ibandl.htm

[21] Jash, R. (2022). *A Study of Stars - Structure and Evolution* [Master's Dissertation, St. Xavier's College (Autonomous), Kolkata]

[22] Kundalia, K. (2024). *Study of α-Cluster Transfer Reactions with ^{7}Be* [Doctoral Thesis, University of Calcutta]

[23] Lane, A.M., Thomas, R.G. *R-Matrix Theory of Nuclear Reactions.* Reviews of Modern Physics, Vol 30, Number 2 Part 1 (1958).

[24] Azuma, R. *et al.*, *AZURE, An R-Matrix Computer Code.* Proceedings of Science. https://pos.sissa.it/053/204/pdf

[25] Sen, S. *Resonance analysis using R Matrix- a cookbook.*

[26] *TUNL Nuclear Data Project.*Nuclear Data group, Triangle Universities Nuclear Laboratory. Accessed on 1st April, 2025 from https://nucldata.tunl.duke.edu/

[27] Cannon, A.J., Pickering, E.C. *Henry Draper Catalog and Extension: III/135A.* Accessed on 1st April, 2025 from https://cdsarc.u-strasbg.fr/viz-bin/Cat?III/135A

[28] Buchmann, L.R., Barnes, C.A., *Nuclear reactions in stellar helium burning and later hydrostatic burning stages.* Nuclear Physics A, Volume 777,Pages 254-290, ISSN 0375-9474. (2006). https://doi.org/10.1016/j.nuclphysa.2005.01.005

[29] Paxton, B., Bildsten, L., Dotter, A., Herwig, F., Lesaffre, P., and Timmes, F. *Modules for Experiments in Stellar Astrophysics (MESA).* The Astrophysical Journal Supplement Series, vol. 192, no. 1, Art. no. 3, IOP, (2011). doi:10.1088/0067-0049/192/1/3.